Check for updates

Bioactive Suture with Added Innate Defense Functionality for the Reduction of Bacterial Infection and Inflammation

Manoj Puthia, Jitka Petrlova, Ganna Petruk, Marta Butrym, Firdaus Samsudin, Madelene Å Andersson, Ann-Charlotte Strömdahl, Sebastian Wasserstrom, Erik Hartman, Sven Kjellström, Lucrezia Caselli, Oxana Klementieva, Peter J. Bond, Martin Malmsten, Deepak Bushan Raina, and Artur Schmidtchen*

Surgical site infections (SSI) are a clinical and economic burden. Suture-associated SSI may develop when bacteria colonize the suture surface and form biofilms that are resistant to antibiotics. Thrombin-derived C-terminal peptide (TCP)-25 is a host defense peptide with a unique dual mode of action that can target both bacteria and the excessive inflammation induced by bacterial products. The peptide demonstrates therapeutic potential in preclinical in vivo wound infection models. In this study, the authors set out to explore whether TCP-25 can provide a new bioactive innate immune feature to hydrophilic polyglactin sutures (Vicryl). Using a combination of biochemical, biophysical, antibacterial, biofilm, and anti-inflammatory assays in vitro, in silico molecular modeling studies, along with experimental infection and inflammation models in mice, a proof-of-concept that TCP-25 can provide Vicryl sutures with a previously undisclosed host defense capacity, that enables targeting of bacteria, biofilms, and the accompanying inflammatory response, is shown.

1. Introduction

Of more than 300 million surgical procedures performed worldwide annually,[1] almost 10% develop surgical site infections (SSIs).[2] SSIs account for a substantial clinical and economic burden.[3] Although many factors contribute to SSIs, preventive measures before, during, and after surgery can lower the SSI incidence.[4] Causes of SSIs vary depending on anatomy, surgical procedure, and exogenous in addition to endogenous, patient-derived factors. Bacterial contamination is one cause that can be controlled.[4,5] In hospitals, preventive measures such as hygiene routines are implemented but even under sterile surgical conditions, infections may occur due to the spread of bacteria from the patient's own bacterial flora.[6] It has also been reported

M. Puthia, J. Petrlova, G. Petruk, M. Butrym, M. Å Andersson,
A.-C. Strömdahl, E. Hartman, A. Schmidtchen
Division of Dermatology and Venereology
Department of Clinical Sciences
Lund University
Lund SE-22184, Sweden
E-mail: manoj.puthia@med.lu.se

F. Samsudin, P. J. Bond
Bioinformatics Institute (BII)
Agency for Science
Technology and Research (A*STAR)
Singapore 138671, Singapore

S. Wasserstrom
Lund University Bioimaging Centre
Lund University
Lund SE-22184, Sweden

S. Kjellström
Division of Mass Spectrometry
Department of Clinical Sciences
Lund University
Lund SE-22184, Sweden

L. Caselli, M. Malmsten
Physical Chemistry 1
Lund University
Lund S-221 00, Sweden

O. Klementieva
Medical Microspectroscopy Lab
Department of Experimental Medical Sciences
Faculty of Medicine
Lund University
Lund SE-221 84, Sweden

P. J. Bond
Department of Biological Sciences
National University of Singapore
Singapore 117543, Singapore

M. Malmsten
Department of Pharmacy
University of Copenhagen
Copenhagen DK-2100, Denmark

**ADVANCED
SCIENCE NEWS**

www.advancedsciencenews.com

**ADVANCED
HEALTHCARE
MATERIALS**

www.advhealthmat.de

that up to 60% of the bacteria recovered from infected surgical wounds developed antibiotic resistance.[7]

During surgery, a variety of sutures is used. These sutures are constructed for different purposes. Vicryl (a hydrophilic polyglactin polymer) is a synthetic absorbable suture used for soft tissue approximation and ligation.[8] Vicryl (polyglactin 910) consists of a copolymer poly(L-lactide-co-glycolide) (10:90 ratio). Vicryl sutures are degraded in the tissues and absorbed.[9] They are the most widely used sutures worldwide and are used for both internal and skin surgeries.[10] Sutures provide an ideal surface for bacteria to adhere to and grow and may be involved in the development of SSI pathogenesis.[11] Therefore, efforts have been made to functionalize sutures to prevent bacterial colonization and consequent infection.[12] Common anti-infective sutures containing antiseptic molecules such as triclosan have however shown inadequate efficacy and may induce bacterial resistance.[13,14] In addition, triclosan can cause side effects, such as hormonal disruption in addition to causing resistance problems.[14]

Nature has developed powerful natural mechanisms to facilitate proper wound healing and bacterial control. Based on our discovery of thrombin-derived C-terminal peptides (TCP) in wounds,[15] we have developed thrombin-derived C-terminal peptide (TCP)−25, a new peptide-based drug with a dual mode-of-action[16] and proven therapeutic potential for the treatment of wound infections.[17,18] TCP-25 binds bacterial lipopolysaccharide (LPS) and interacts directly with monocytes and macrophages.[19] It inhibits cluster of differentiation (CD)−14-mediated Toll-like receptor (TLR)-induced nuclear factor kappa beta (NF-κB) activation, which occurs in response to various agonists of microbial origin and intact bacteria. TCP-25 binds to LPS and also exhibits a high affinity binding to the LPS binding pocket of CD14, the main receptor for LPS.[16] A TCP-25 hydrogel formulated using a neutral polymer (hydroxyethyl cellulose, HEC) was shown to reduce both wound bacteria and harmful excessive inflammation.[17] Importantly, TCP-25 was found not to bind to the HEC polymer, which is crucial for maintaining its action in the hydrogel and enabling fast release into the wound environment. The hydrogel showed efficacy against *Staphylococcus aureus* and *Pseudomonas aeruginosa* and was therapeutically used in mouse and porcine wound infection models.[17] Moreover, TCP-25 retained its dual function when incorporated into a polyurethane wound dressing.[18] Thus, therapies based on TCP-25 boosting of natural defenses represent a promising approach for wound healing.

Given these promising data on wound infections; it remains, however, to be investigated whether sutures could be functionalized with TCP-25. Moreover, as sutures remain at the surgical site for a longer duration, we reasoned that interaction between TCP-25 and suture material should be advantageous for sustained efficacy. This prompted us to study the binding of TCP-25 to the Vicryl polymer and explore whether, by reducing localized infection-inflammation, TCP-25 could provide a new, pharmacologically well-defined functionality to Vicryl sutures. If successful, this proof-of-concept would provide novel opportunities within the surgical area; thus, improving outcomes. In this context, we wanted to investigate if localized delivery of TCP-25 from Vicryl sutures could offer a new method for reducing both bacteria and the associated inflammation. Here, we provide a detailed molecular characterization of the interaction between TCP-25 and the polyglactin 910 copolymer and its functional significance. Using a comprehensive combination of in silico, in vitro, and in vivo assays, we demonstrate a proof-of-concept that TCP-25 provides Vicryl sutures with a "dual-function" capability that targets both bacteria and the associated inflammation.

2. Results and Discussion

2.1. Characterization of Peptide Release from TCP-25-Coated Polyglactin Sutures

In order to retain the antimicrobial and anti-inflammatory effects of TCP-25, we decided to use a reductionist approach, avoiding added formulation components for this proof-of-concept work. Hence, TCP-25 was used for coating of polyglactin sutures using a simple method involving submerging the suture in TCP-25 peptide solution, followed by drying. To determine optimal coating conditions, sutures were kept in a 0.1%, 0.5%, 2.0%, and 4.0% TCP-25 solution for 2 h; and subsequently, air dried. The peptide was then eluted from the sutures, and peptide concentration was determined. Sutures coated with 2% TCP-25 solution showed significantly higher peptide recovery (**Figure 1**a, left panel). Sutures coated with 4% TCP-25 solution did not exhibit better TCP-25 recovery than those coated with a 2% solution possibly due to oligomerization of TCP-25 molecules at high concentrations, as reported previously.[20] Radial diffusion assay (RDA) was used to analyze the release and antimicrobial activity of the eluted peptide, and the results showed that sutures coated with 2% TCP-25 showed the highest antimicrobial activity (Figure 1a, right panel). A TCP-25 coating concentration of 2% was therefore found to be optimal. Next, the influence of coating time and temperature on the suture peptide content and antibacterial capacity was investigated. Coating times of 1, 2, 4, 8, and 24 h all yielded similar TCP-25 recovery from the sutures (Figure 1b, left panel). Correspondingly, using RDA, the zones of inhibition for 1, 2, 4, and 8 h coating times were determined. Although the differences between the time points were small, the zone of inhibition for the 2-h coating time was relatively higher than other coating times (Figure 1b, right panel). Sutures coated at temperatures of 21 °C showed relatively higher TCP-25 recovery than the sutures coated at 37 °C and 50 °C (Figure 1c, left panel). All coating temperatures showed no apparent effect on the antibacterial activity as similar zones of inhibition were observed in RDA (Figure 1c, right panel). Upon SDS-PAGE analysis of the peptide eluted from the sutures, no degradation of TCP-25 was observed for the various coating times and temperatures (Figure S1, Supporting Information). Moreover, suture TCP-25 loading was investigated at coating concentrations of

D. B. Raina
Department of Clinical Sciences Lund
Orthopedics
Faculty of Medicine
Lund University
Lund SE-221 84, Sweden
A. Schmidtchen
Dermatology
Skane University Hospital
Lund SE-22185, Sweden
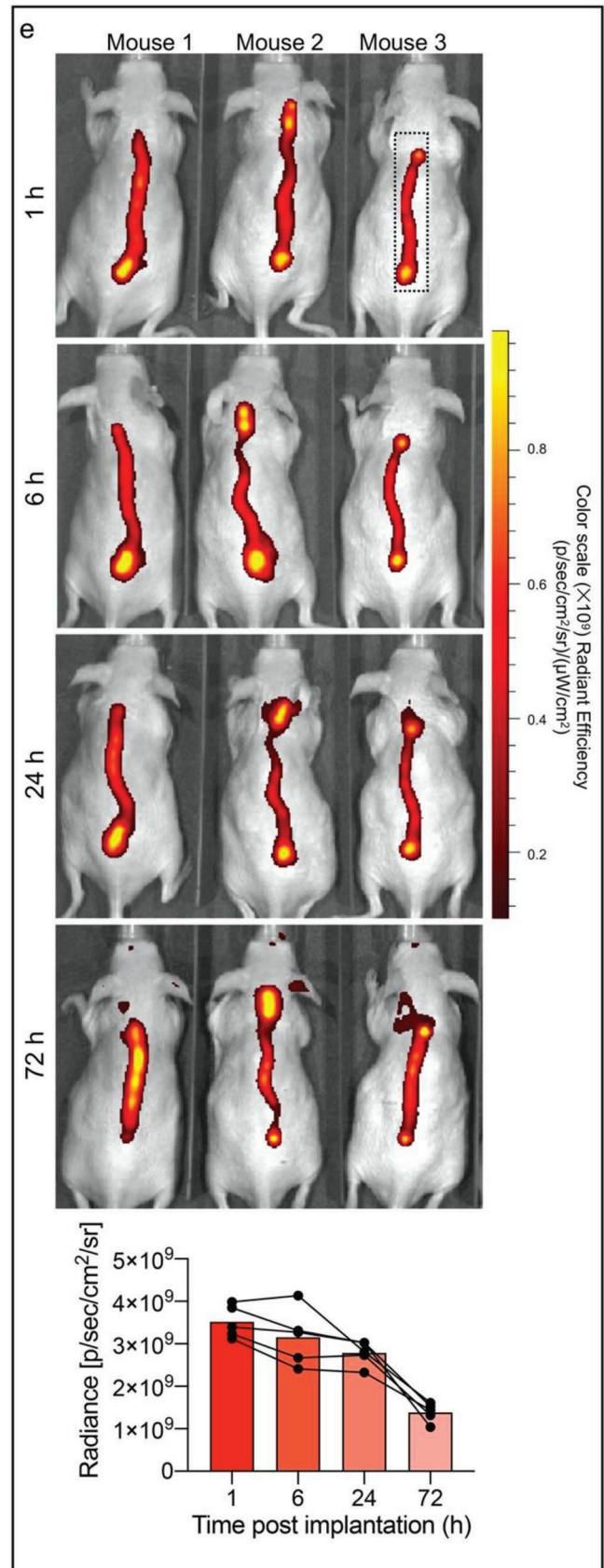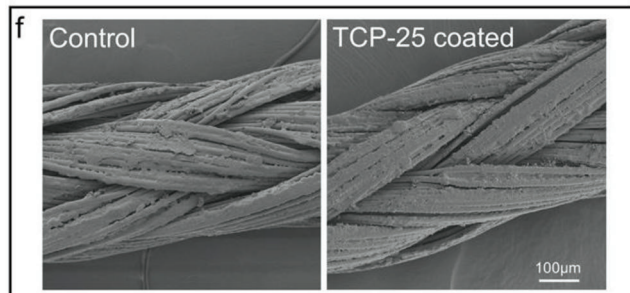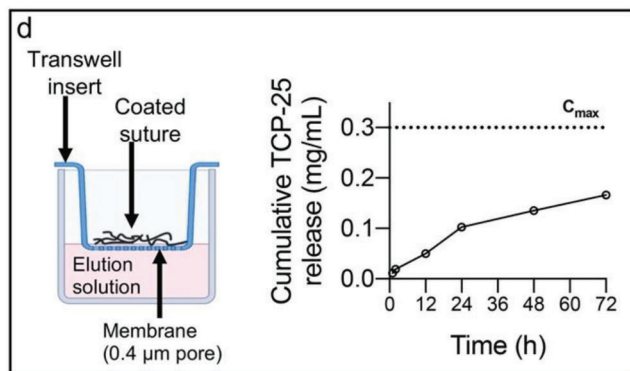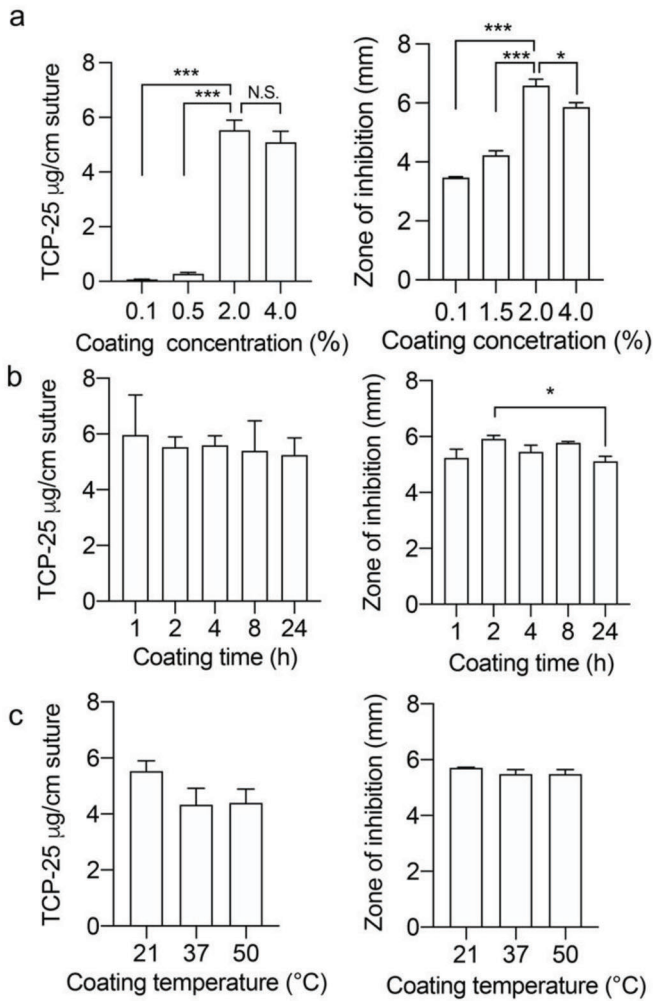
0.5%, 2.0%, and 4.0% (Figure S2, Supporting Information). A coating concentration of 0.5% TCP-25 solution resulted in low loading efficiency, while a 2% coating concentration showed significantly higher suture TCP-25 loading efficiency. Interestingly, a 4% coating concentration exhibited suture TCP-25 loading efficiency similar to that of a 2% coating concentration. Based on the results, a 2% coating concentration for 2 h at 21 °C was selected as the final coating condition for the experiments in this project.

Next, to assess peptide release from the suture, we first used an in vitro model.[21] A Transwell filter insert system was employed, and TCP-25 sutures were kept on the porous filter in the apical compartment. Elution buffer was added to fill the basolateral compartment. The elution buffer was in contact with the filter and the TCP-25 suture (as illustrated in Figure 1d). After a quick release for the initial 24 h, continuous TCP-25 release was observed for 72 h (Figure 1d). Hairless SKH-1 mice were used to further study the in vivo release of TCP-25 from sutures. Sutures were coated with TAMRA-labeled TCP-25 and subcutaneously implanted. Longitudinal fluorescent bioimaging was then performed using the IVIS spectrum in vivo imaging system. Release of the peptide was observed in the immediate implant surroundings and most of the peptide appeared to be retained locally in and around the suture (Figure 1e). TCP-25 TAMRA fluorescent intensity was observed after 1 h, which gradually decreased over time, but significant signals were acquired even 72 h after the implantation (Figure 1e, bar chart). Finally, surface morphological characteristics of the uncoated control and TCP-25-coated sutures were studied by scanning electron microscopy (SEM). A typical braided structure of polyglactin sutures was observed in both control and coated sutures (Figure 1f). No apparent differences were observed on the surface of TCP-25-coated sutures in comparison to the surface of control sutures.
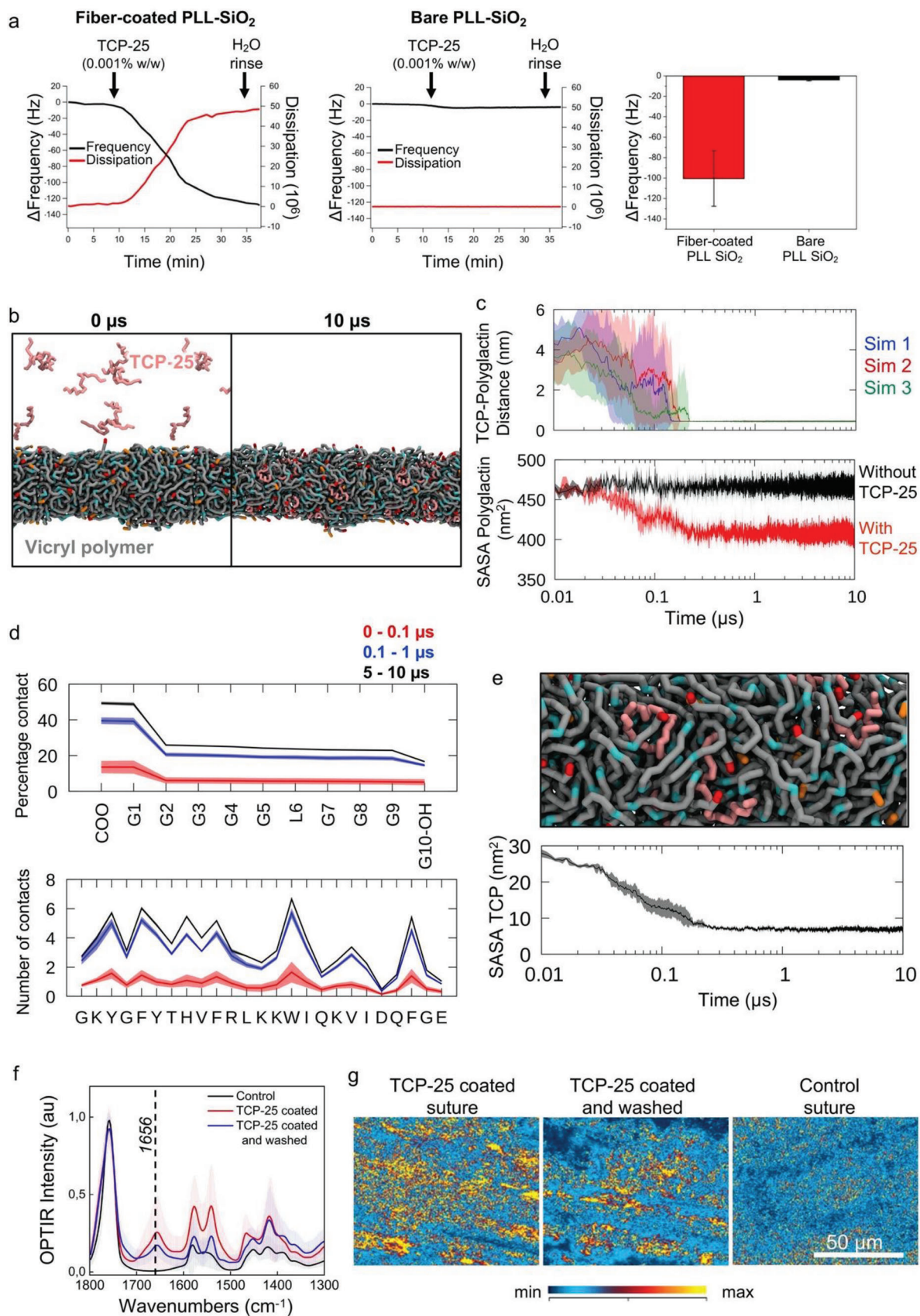
2.2. Characterization of Peptide–Polyglactin Interactions Using QCM-D, In Silico Modeling and Simulation, and O-PTIR Analysis

To investigate the interaction of TCP-25 with Vicryl suture fibers, Quartz Crystal Microbalance with Dissipation Monitoring (QCM-D) was employed. Finely cut suture fibers (50–100 µm) were dispersed into ethanol, and subsequently, drop-cast onto SiO_2-based substrate for QCM-D measurements. To allow precise monitoring of peptide binding to the suture fibers, the underlying SiO_2 surface was modified by poly-L-lysine under low ionic strength, resulting in a thin and net positively charged surface,[22] which has previously been demonstrated to display low adsorption of a range of host defense peptides.[23] Indeed, the cationic poly-L-lysine surface coating was efficient in suppressing the adsorption also for TCP-25, despite the peptide concentration corresponding to plateau in the binding isotherm for other surfaces[24] (**Figure 2a**). In stark contrast, the fiber-coated surfaces displayed very pronounced peptide binding, as seen from the strongly decreasing frequency change (ΔF). Thus, a frequency shift of -100 ± 27 Hz was observed for the fiber-coated surfaces, whereas a mere -4 ± 1 Hz was observed for the underlying poly-L-lysine surface. While a quantitative interpretation of these results in terms of the amount of peptide bound to the fiber is not possible due to the uncertainty of the fiber surface area as well as of the amount of solvent oscillating with the crystal during measurement, it is nevertheless clear that the peptide binding to and affinity for the suture fibers is high, much higher than typically found for host defense peptides binding to bare SiO_2 surfaces.[25] Finally, we note that the kinetics for peptide binding is relatively slow (in line with the release results discussed above), and that initiation of rinsing after peptide loading does not result in an immediate peptide release; both effects suggest that peptide binding occurs not only on the outer surface of the fibers but also in pores and defects.

To understand the molecular mechanism underlying the interaction between TCP-25 with polyglactin sutures, we built a coarse-grained (CG) model of polyglactin 910 copolymer comprised of 90% glycolide and 10% lactide subunits; parameters were developed within the Martini forcefield framework based on atomic-resolution sampling, as described in in silico modelling and simulations section in Materials and Methods (Figure S3, Supporting Information). We simulated the spontaneous self-aggregation of the polymers made of 100-mer chains; and then, added ten copies of TCP-25 peptides (details in Material and Methods). The peptides rapidly adsorbed to the surface of the polyglactin polymer (Figure 2b). In less than 200 ns, all peptides in the system were interacting with the polymer (Figure 2c, top), leading to progressive burial of the polymer's solvent accessible surface area (SASA) (Figure 2c, bottom). Contact analysis indicates that the negatively charged carboxyl termini of the polyglactin polymer chains interact the most with the cationic peptides (Figure 2d, top). Interestingly, we observed that once the peptides have adsorbed to the outer surface of the polymer, they become entangled with the polymer chains and gradually integrate into the polymer phase (Figure 2e), in agreement with the QCM-D results described above. This is evidenced by the dramatically reduced SASA of the TCP-25 peptides during the simulations. Polar (Y3, Y6, H8) and hydrophobic (F5, F10, W15, F23) residues play an important role in peptide integration into the polymer phase (Figure 2d, bottom).

Figure 1. Coating conditions, antibacterial properties, and release profile of TCP-25 peptide-coated polyglactin suture. Effects of coating conditions on the peptide loading and antimicrobial activity of polyglactin sutures. Sutures were coated with TCP-25 under a) varying conditions of coating concentrations, b) coating times, and c) coating temperatures. The peptide was eluted from the coated sutures, and protein concentrations were estimated (left panels). To study effects on antimicrobial activity, elutions from sutures were used in a radial discussion assay (RDA) as shown in the right panel. The diameter of the clear zone (excluding the 4 mm well) was presented as the inhibitory effect of the released peptide (For [1a,b,c], mean values ± standard error of the mean [SEM] are presented, $n = 3$). d) The cumulative release of TCP-25 from sutures in vitro. As illustrated, a Transwell insert was used to obtain conditions mimicking a surgical wound, and TCP-25 release was estimated. e) In vivo release of TCP-25 from suture. In SKH-1 mice, sutures coated with tetramethylrhodamine (TAMRA)-labeled TCP-25 were subcutaneously placed. At 1, 6, 24, and 72 h, peptide release was longitudinally monitored by quantifying fluorescence using IVIS imaging. Heat map overlays obtained from emitted light are shown. Bar chart shows the measured radiance emitted from the region of interest (mean values are presented, $n = 4$). The dotted line shows the region of interest. f) Scanning electron microscopy showing the surface of the polyglactin sutures before and after the TCP-25 coating. $*P \leq 0.05$ and $***P \leq 0.001$.

2300987 (5 of 20)

ADVANCED
SCIENCE NEWS
www.advancedsciencenews.com

ADVANCED
HEALTHCARE
MATERIALS
www.advhealthmat.de

At a higher peptide concentration, we saw slower overall peptide adsorption, likely due to peptide aggregation in solution prior to binding (Figure S4a, Supporting Information), which aligns with the experimental results obtained using different coating concentrations above. At shorter chain length (50-mer), we found no difference in the ability of the peptides to integrate into the polymer phase (Figure S4b, Supporting Information). At physiological temperature (310 K) and room temperature (298 K), we found marginally slower rates of peptide absorption; however, the peptides reached a similar SASA value by the end of the simulations, indicating that lower temperatures do not significantly affect the ability of the peptide to be integrated into the polymer (Figure S4c, Supporting Information). We also found that the binding of peptides to the polyglactin polymer displaced Na^+ ions on the polymer surface, further highlighting the interaction between the peptides and the carboxyl groups of the polymer (Figure S4d, Supporting Information). While we observed aggregation of peptides in solution and on the surface of the polymer, the peptides disaggregated once integrated into the polymer phase (Figure S4e, Supporting Information). Collectively, our results agree with previous experimental studies of poly-lactic-co-glycolic acid (PLGA) interaction with cationic peptides, whereby the peptides not only bind on the surface but can also be integrated and distributed within the polymer phase.[26] This may explain the retained bioactivity upon long-term storage of TCP-25 sutures.

To further validate the interaction of TCP-25 with Vicryl sutures, optical photothermal infrared (O-PTIR) spectroscopy measurements were performed on uncoated and TCP-25-coated sutures. Spectral analysis shows the presence of a new band at 1665 cm^{-1} in coated sutures indicating the presence of TCP-25 on the fibrils (Figure 2f,g; Figure S5, Supporting Information). Importantly, 30 min washing of sutures in water does not significantly affect the newly formed band further supporting the interaction of TCP-25 with the suture. Finally, fluorescence imaging of cryosections of sutures coated with TCP-25-Cy3 revealed the distribution and localization of TCP-25 on suture fibrils (Figure S6, Supporting Information). TCP-25 appears to be intensely distributed on the surface and in between Vicryl fibrils.

2.3. Peptide Structure and Function Analysis

Interaction of peptides with other materials might have deleterious effects on their structure and function. To study if the coating of polyglactin suture with TCP-25 affects peptide structure and activity, we analyzed TCP-25 eluted from the coated sutures using high-performance liquid chromatography (HPLC). No difference in the main peptide elution pattern was observed, indicating that the coating procedure had no apparent effect on peptide stability (**Figure 3**a). The capability of TCP-25 to bind to LPS and neutralize it is paramount to its anti-inflammatory activity. We further investigated whether TCP-25 retains its capability to interact with and bind to LPS after coating. The peptide was eluted from the coated suture, and in the presence of LPS, structural changes in the presence of LPS were studied with circular dichroism (CD) analysis. Results indicated that TCP-25 eluted from the coated sutures showed a similar change in α-helix induction as observed for the control peptide, a finding that indicates compatibility with the interaction between TCP-25 and LPS (Figure 3b). Upon excitation at 280 nm, alteration in peptide's intrinsic fluorescence was determined by the LPS-induced structural change. LPS-peptide binding was observed and indicated by a blue-shift in emission maximum (λ_{max}) (Figure 3c) as determined by fitting the Δ_{max} of TCP-25 in the function of varying concentrations of LPS. A K_d of 11.15 ± 1.76 µg mL^{-1} was observed, which is in agreement with previous results (Figure 3d).[18]

2.4. Antibacterial Properties and Efficacy of TCP-25-Coated Sutures In Vitro and in an Experimental Mouse Model of Suture Infection

We used several in vitro assays to determine the antimicrobial efficacy of the TCP-25-coated sutures. Bioluminescent *S. aureus* and *P. aeruginosa* were used to demonstrate antibacterial efficacy. Compared to control sutures, bacteria treated with TCP-25-coated sutures showed a significant reduction in bioluminescence as visualized by IVIS bioimaging. This effect was already observed 5 min after addition of the TCP-25 sutures, showing the release and rapid antibacterial effects of TCP-25

Figure 2. QCM-D, coarse-grained simulation, and O-PTIR analysis showing peptide–polyglactin interactions. a) QCM-D monitoring of TCP-25 binding to Vicryl fibers. Finely cut fibers were dissolved in ethanol and drop-cast to poly-L-lysine-coated SiO2 to a confluent fiber mat. Peptide binding onto fiber-functionalized sensors was confirmed by frequency changes (ΔF) of −100 ± 27 Hz and dissipation changes (ΔD) of (+42 ± 11) × 10^{-6}, with respect to pure MQ water. In contrast, the possible adsorption of the peptide onto the underlying poly-L-lysine surface was ruled out in control experiments, in which the interaction of the peptide with fiber-free poly-L-lysine-functionalized SiO2 surfaces was monitored under the same experimental conditions, showing only a minute frequency shift of −4 ± 1 Hz. Measurements were performed at room temperature (*n* = 3). b–e) Coarse-grained simulations of Vicryl assembly with TCP-25. A 1 µs CG self-assembly simulation of 50 copies of the 100-mer polyglactin 910 model was performed to build a Vicryl polymer model. Subsequently, ten copies of TCP-25 were added to the system and three independent 10 µs simulations were conducted at 320 K. The figure shows initial and final snapshots from one of the simulations. Polyglactin chains are coloured cyan (lactic acid subunits), grey (glycolic acid subunits), red (carboxyl terminus), and orange (hydroxyl terminus). The TCP-25 peptides are shown in pink (b). (Top) Minimum distance between TCP-25 peptides and the surface of the Vicryl polymer for all three simulations. Thick lines show average over ten peptides and the shaded areas indicate standard deviation. (Bottom) Solvent accessible surface area (SASA) of the Vicryl polymer comparing simulation with (red) and without (black) TCP-25. Thick lines show average over three repeat simulations and shaded areas indicate standard deviation. Probe radius used for SASA calculation is 0.26 nm (c). (Top) The average percentage of contacts made by each subunit of polyglactin with the peptide at three time points during the simulations. COO, carboxyl terminus; G1 to G9, glycolide subunits; L6, lactide subunit; and G10-OH, glycolide with hydroxyl terminus. (Bottom) The same analysis performed for each residue of the peptide. Distance cut-off used for contact measurement was 0.6 nm (d). (Top) An enlarged snapshot showing entanglement of the TCP-25 peptide with the polyglactin polymer from the end of one simulation. (Bottom) SASA of the peptides throughout the simulations, averaged over ten peptides and three simulations (e). f) Normalized O-PTIR spectra acquired at 2 cm^{-1} spectral data point spacing with five averages from uncoated (control), TCP-25 coated, and washed TCP-25 coated sutures. Dashed line shows the band position characteristic for TCP-25 coated sutures at 1656 cm−1. g) O-PTIR ratio maps were derived from the images acquired at 1656 cm^{-1} (ratio map nominator) and divided by the images acquired at 1760 cm^{-1} (ratio map denominator). The yellow color shows the distribution of TCP-25 on the suture surface.

2300987 (6 of 20)

**ADVANCED
SCIENCE NEWS**

www.advancedsciencenews.com

**ADVANCED
HEALTHCARE
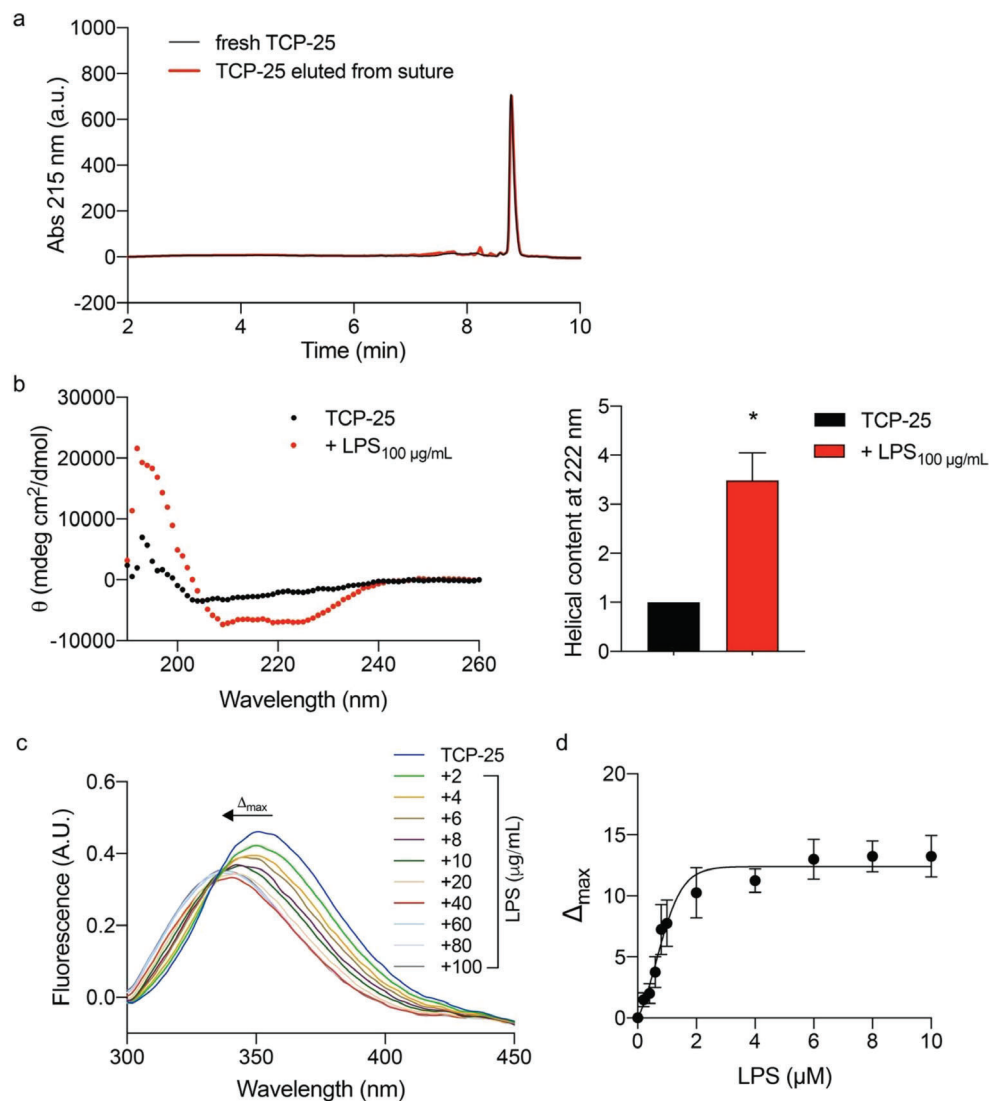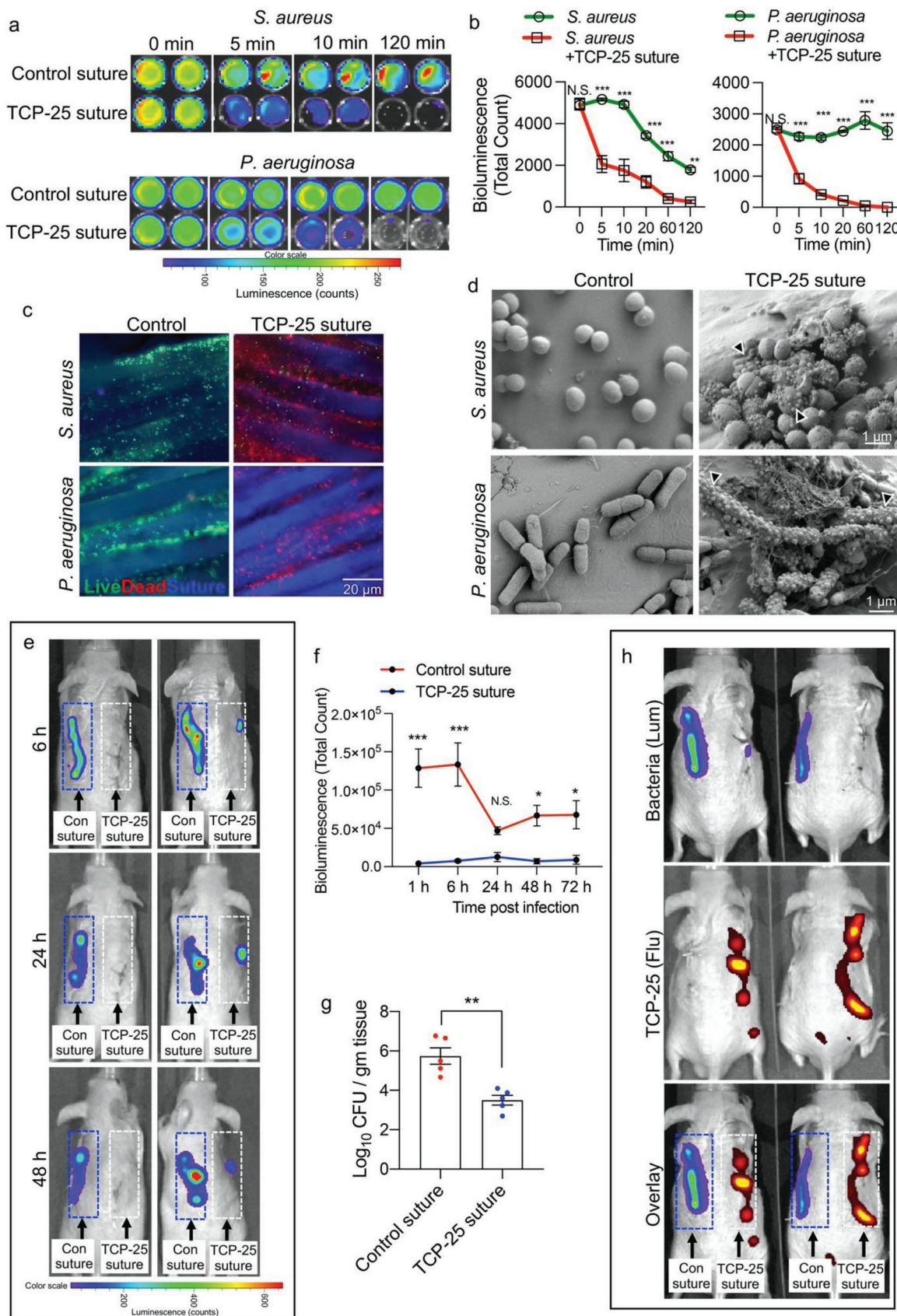MATERIALS**

www.advhealthmat.de

Figure 3. Structural analysis of TCP-25 eluted from coated sutures. a) High-performance liquid chromatography (HPLC) analysis of fresh TCP-25 or TCP-25 eluted from coated sutures. b) Circular dichroism (CD) spectra of TCP-25 from coated sutures either alone or after incubation with LPS (left panel). The α-helical content of TCP-25 estimated from molar ellipsometry at 222 nm (right panel) is displayed. Data are presented as the mean $\pm$ SEM ($n = 3$). P values were determined using an unpaired t-test. c) Intrinsic fluorescence spectra of 10 μM TCP-25 from the coated sutures, showing shifts in the emission maximum of the peptides after incubation with varying concentrations of LPS (left panel). d) Fitting of the TCP-25's emission maximum wavelength (Δmax) in function of varying concentrations of LPS. Data are represented as the mean $\pm$ SEM ($n = 3$). *$P \leq 0.05$.

(**Figure 4**a). In another experiment using bioluminescent bacteria, with a luminometer, luminescence was measured after the addition of sutures. A rapid and consistent decrease in bacterial luminescence was observed after the addition of TCP-25-coated sutures (Figure 4b). Next, a live–dead assay was employed to study membrane integrity. The analyses showed that only the TCP-25-coated sutures yielded significant permeabilization of *S. aureus* and *P. aeruginosa* bacteria (Figure 4c). SEM was used to further study the effects of TCP-25-coated sutures on bacterial morphology. Bacteria adhering to TCP-25-coated sutures showed significant morphological changes, such as bacterial lysis and clumping, and the presence of debris was observed (Figure 4d). In contrast, smooth and normal cell wall surfaces were observed on bacteria in the control suture group. Overall, these results

show that TCP-25 holds its rapid antibacterial activity even after being coated on the polyglactin sutures.

Next, to answer whether TCP-25-coated sutures maintain antibacterial efficacy in vivo, we employed an experimental mouse model of suture infection mimicking a situation of clinical SSIs. *S. aureus* was chosen for in vivo experiments due to its significant relevance to SSIs.[27] Control or TCP-25-coated sutures were subcutaneously implanted into the left or right side of the BALB/c mice and contaminated with bioluminescent *S. aureus*. IVIS spectrum was used for non-invasive longitudinal in vivo bioimaging of the infection. A significant decrease in bioluminescence intensity was observed at the TCP-25-coated suture side when compared with the control side (Figure 4e). Bioluminescence measurement showed that bacterial infection persisted around the

**ADVANCED
SCIENCE NEWS**

www.advancedsciencenews.com

**ADVANCED
HEALTHCARE
MATERIALS**

www.advhealthmat.de

**ADVANCED
SCIENCE NEWS**

www.advancedsciencenews.com

**ADVANCED
HEALTHCARE
MATERIALS**

www.advhealthmat.de

control suture site, whereas TCP-25-coated sutures kept the infection significantly low throughout the experiment and even until the last observed time point of 72 h (Figure 4f). At the 72 h endpoint, analysis of the tissue around the suture site showed that TCP-25-coated sutures caused a significant reduction in numbers of bacteria (Figure 4g). To visualize the distribution of TCP-25 and further confirm that antibacterial effects were indeed due to the TCP-25-coated suture, fluorescently-labeled TCP-25 (TCP-25-TAMRA) was used for the coating; then, subcutaneously implanted and contaminated with *S. aureus*. We observed that TCP-25-coated sutures inhibited bacterial growth and TCP-25 fluorescence co-localized with the suture site (Figure 4h). To investigate further if TCP-25 coated sutures exhibit in vivo antibacterial efficacy against *Escherichia coli*, sutures were contaminated with CLSI control strain *E. coli* (ATCC 25922), and tissue around the suture site was analyzed at 72 h. CFU determination showed that TCP-25-coated sutures caused a significant reduction in number of bacteria (Figure S7, Supporting Information).

2.5. In Vitro and In Vivo Effects of TCP-25-Coated Suture on Endotoxin Responses

We further investigated the anti-inflammatory efficacy of TCP-25-coated sutures employing in vitro and in vivo models. A reporter assay employing THP1-XBlue-CD14 cells was used. LPS with or without TCP-25 from coated sutures was used to stimulate reporter cells. A significant reduction in endotoxin-induced NF-κB and AP-1 activation was observed in the presence of TCP-25 eluted from sutures (**Figure 5**a, upper panel). Results from MTT assay showed that these concentrations of TCP-25 were not toxic to the cells (Figure 5a, lower panel).

Next, it was important to know whether TCP-25-coated sutures show similar anti-inflammatory efficacy in vivo. To study this effect, we used an NF-κB reporter mouse model in which the suture was subcutaneously implanted and contaminated with LPS followed by longitudinal in vivo inflammation bioimaging using IVIS spectrum. A high level of local NF-κB activation was observed at the side at which the non-coated control suture was implanted. In contrast, TCP-25-coated sutures led to a significant reduction in this NF-κB-driven inflammation at 3 and 24 h after suture implantation (Figure 5b). At the end of the experiment, we recovered the sutures from the mice and eluted absorbed proteins for cytokine analysis. A significant reduction in

TNF-α and IL-6 cytokine levels in fluid extracted from implanted TCP-25-coated sutures was observed compared to the control sutures (Figure 5c).

2.6. Effects of TCP-25-Coated Sutures on Bacterial Biofilm

To investigate whether the TCP-25-coated sutures possess anti-biofilm effects, we used two different experimental approaches. In the first approach, our aim was to evaluate the impact of TCP-25 coating of the suture on the growth of biofilms in the microtiter plate wells and on the sutures themselves. To achieve this, 30 min after the addition of bacteria, control or TCP-25-coated sutures were added to the wells of the microtiter plate during the biofilm growth. Biofilms were allowed to grow at 37 °C. After 48 h, live/dead staining, bacterial count of the suture-attached biofilm, and crystal violet staining of the microtiter plate attached biofilm were performed. Under a fluorescence microscope after live–dead staining, bacterial biofilm formation (green staining) on the sutures was visible for both *S. aureus* and *P. aeruginosa* (**Figure 6**a). On the TCP-25-coated sutures, less biofilm formation and red staining indicating the presence of dead bacteria, were visible. A viable count assay was used to assess the total number of live bacteria on suture-adhered biofilm. TCP-25-coated sutures showed significantly lower bacterial numbers (Figure 6a, bar chart). Likewise, crystal violet staining of the plate showed a significantly lower amount of biofilm formation in the wells containing TCP-25-coated sutures. Importantly, comparison with a benchmark antibacterial suture (Vicryl Plus) containing triclosan showed similar antibiofilm activity against *S. aureus*, but its activity against *P. aeruginosa* biofilm formation was not significant (Figure 6a,b). Finally, SEM of the sutures showed a significantly lower amount of adhered biofilm on the TCP-25-coated sutures (Figure 6c).

In the second approach, the aim was to study the impact of TCP-25-coated sutures on mature biofilms. *S. aureus* or *P. aeruginosa* biofilms were grown on the plate and exposed to TCP-25-coated sutures for 2 h. Live/dead staining showed a significant increase in dead bacterial cells (red-stained) in the samples exposed to TCP-25-coated sutures (Figure 6d,e). As expected, the viable count assay of the biofilms exposed to TCP-25-coated sutures showed a significant reduction in bacterial numbers (Figure 6d,e, bar charts). Benchmark triclosan-containing sutures showed comparable antibiofilm activity against *S. aureus*,

Figure 4. In vitro and in vivo antibacterial effects of TCP-25 suture. a) Bioluminescent *S. aureus* or *P. aeruginosa* bacteria were incubated with TCP-25-coated or control suture and imaged using IVIS. Representative photos are shown ($n = 3$). b) Bioluminescence emitted from bacteria after treatment with TCP-25 sutures. Bioluminescent versions of *S. aureus* or *P. aeruginosa* were incubated with TCP-25 sutures. Signals from bacteria were acquired using a luminometer. Data are presented as the mean ± SEM ($n = 3$). P values were calculated using a two-way analysis of variance (ANOVA) and Tukey's post hoc test. c) Representative images showing results from Bacterial live–dead assay. Staining was performed using a LIVE/DEAD Baclight bacterial viability kit and imaged using fluorescence microscopy. The green color showed live bacteria whereas the red color showed dead bacteria ($n = 3$). d) Scanning electron microscopy (SEM) images showing the bacterial morphology after contact with TCP-25 sutures. e) In vivo infection imaging showing anti-bacterial properties of TCP-25 sutures in a mouse model of suture infection. Uncoated control sutures or TCP-25 sutures were subcutaneously implanted on the left or right side, respectively and contaminated with bioluminescent *S. aureus*. Bacterial bioluminescence was non-invasively imaged using the IVIS imaging system. f) The line chart shows the bacterial bioluminescence emission at 1, 6, 24, 48, and 72 h post-infection. Data are shown as the mean ± SEM ($n = 5$). P values were calculated using a two-way ANOVA with Sidak's test. g) Bar-chart shows bacterial counts in the tissue surrounding control or TCP-25 sutures. After suture implantation and contamination with *S. aureus*, mice were sacrificed at 72 h and tissue adjacent to the suture was collected for CFU enumeration using viable count assay. Data are shown as the mean ± SEM ($n = 5$ mice per group). P values were calculated using unpaired t-tests. h) In vivo infection and drug imaging by IVIS in mice. To image in vivo drug localization along with bioluminescent bacterial imaging, sutures were coated with fluorescently labeled TCP-25. Representative photos display bioluminescence (lum) and TCP-25 TAMRA fluorescence (flu) 6 h post-suture implantation ($n = 5$). *$P \leq 0.05$; **$P \leq 0.01$; and ***$P \leq 0.001$.
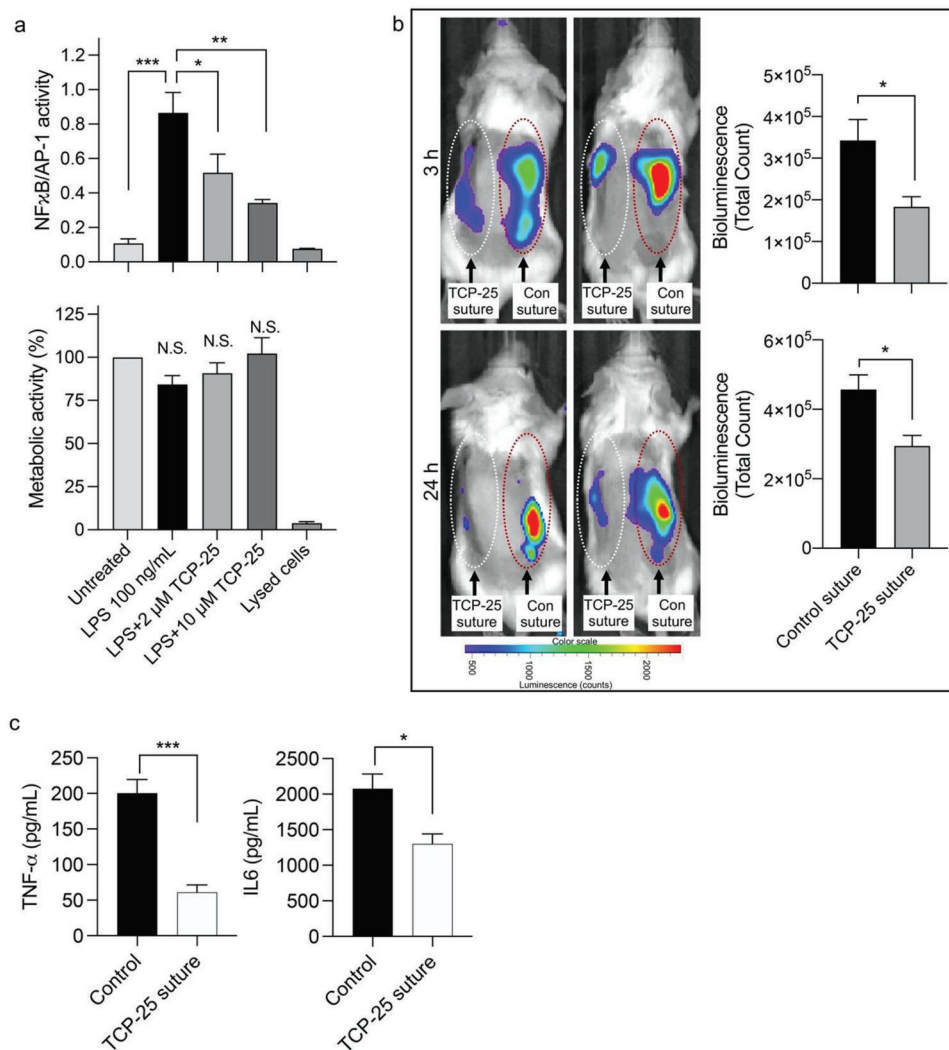
**ADVANCED
SCIENCE NEWS**

www.advancedsciencenews.com

**ADVANCED
HEALTHCARE
MATERIALS**

www.advhealthmat.de

Figure 5. In vitro and in vivo effects of TCP-25 sutures on endotoxin-induced inflammation. a) NF-κB and AP-1 activation analysis by quantifying secreted alkaline phosphatase in THP1-Xblue-CD14 cells (upper bar chart). Cell viability was determined with the MTT assay (lower bar chart). Lysed cells were included as positive control. Data are shown as the mean $\pm$ SEM ($n = 3$). P values were calculated using one-way ANOVA. b) Longitudinal imaging of inflammation in NF-κB reporter mice. TCP-25 or control sutures were implanted on the left or right side, respectively and contaminated with LPS. An IVIS Spectrum system was used for in vivo bioimaging of NF-κB reporter gene expression. Representative heat-map overlay photos show bioluminescent signals at 3 and 24 h after implantation. Bar charts show analysis of the emissions from the NF-κB reporter mice. Data are shown as the mean $\pm$ SEM ($n = 5$). P values were determined using unpaired t-tests. c) TNF-α and IL-6 cytokine levels in fluid extracted from implanted sutures after 24 h of implantation. Data are shown as the mean $\pm$ SEM ($n = 5$ mice per group). P values were calculated by unpaired t-tests. *$P \leq 0.05$, **$P \leq 0.01$, ***$P \leq 0.001$, and ***$P \leq 0.001$. NS: non-significant.

whereas the activity against *P. aeruginosa* biofilm was not significant.

2.7. Effects of Neutrophil Elastase on TCP-25-Coated Suture

Human neutrophil elastase (HNE) is an important enzyme that is produced during wound healing, infection, and inflammation. We have previously demonstrated that HNE digests TCPs in vitro and generates various fragments.[17] It was also shown that HNE can produce active TCP-25 fragments in a TCP-25 hydrogel.[17] We wanted to investigate if HNE could produce bioactive fragments of TCP-25 from a TCP-25-coated suture. TCP-25-coated

sutures were treated directly with HNE after which material was eluted, and the fragmentation pattern was analyzed by nano LC-MS/MS. HNE digestion of TCP-25 that had been coated on the sutures producing numerous peptides at different time points (**Figure 7**a). In addition to fragments, the presence of intact TCP-25 (GKYGFYTHVFRLKKWIQKVIDQFGE) was observed for all the studied time periods. Many of these fragments are known to be bioactive and exert antimicrobial and anti-inflammatory activity.[17] Interestingly, the CD14 binding region was preserved in many of the fragments (Figure 7b). The peptide fragment "cocktail" produced by HNE digestion retained its antibacterial activities for digestion periods of up to 6 h as assessed by RDA (Figure 7c; Figure S8, Supporting Information). In addition, the
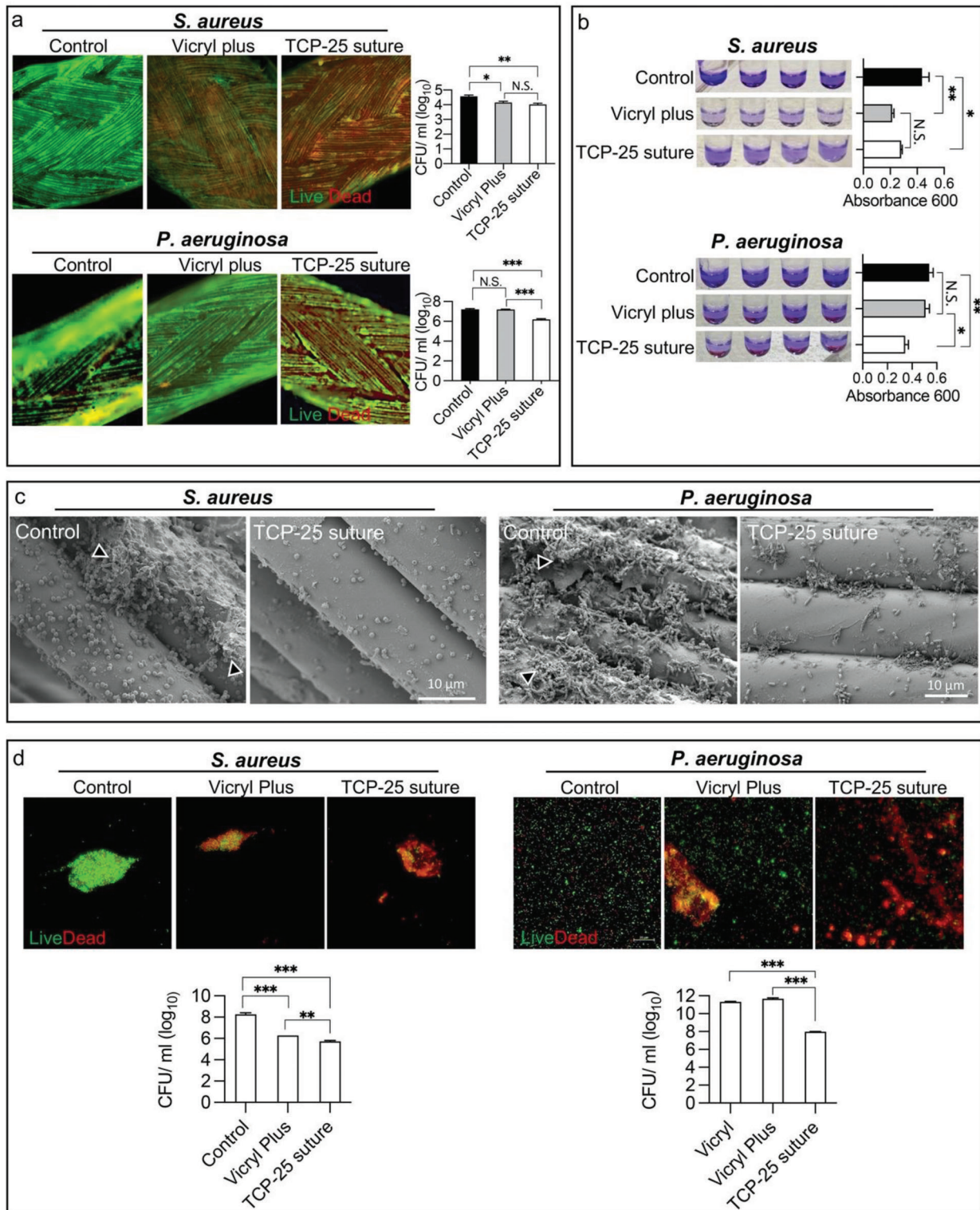
**ADVANCED
SCIENCE NEWS**

www.advancedsciencenews.com

**ADVANCED
HEALTHCARE
MATERIALS**

www.advhealthmat.de

Figure 6. Antibiofilm effects of TCP-25-coated suture. a) Representative fluorescence microscopy images after live/dead staining showing *S. aureus* or *P. aeruginosa* biofilm adhered to the suture surface (green, live bacteria; red, dead bacteria). TCP-25-coated or control sutures were added to the wells of the biofilm microtiter plate, and biofilms were allowed to grow for 48 h. Sutures were stained using LIVE/DEAD Baclight bacterial viability kit and imaged using fluorescence microscopy. Vicryl Plus was used as a benchmark comparison. The bar chart shows the total number of live bacteria on suture-adhered biofilms estimated using a viable count analysis. Data are shown as the mean ± SEM ($n = 3$). P values were analyzed using a one-way ANOVA. b) Crystal violet staining showing measurement of biofilm mass. Vicryl Plus was used as a benchmark comparison. Data are shown as the mean ± SEM ($n = 3$). P values were determined using a one-way ANOVA. c) Scanning electron microscopy of *S. aureus* or *P. aeruginosa* biofilm grown

2300987 (11 of 20)

generated peptide fragments retained their anti-inflammatory activity as observed in THP-1 cell model system (Figure 7d). Overall, the results demonstrated that HNE digestion of TCP-25 from coated sutures produces multiple TCP-fragments and that many of them are bioactive.

2.8. Tensile Strength and Hemolytic Effects of TCP-25-Coated Suture

We next wanted to investigate whether the TCP-25 coating of polyglactin sutures produced any adverse effect on its tensile strength. Mechanical testing of sutures was done using an Instron tensile strength testing system. No change in the tensile strength of the suture was observed after coating with TCP-25 (**Figure 8**a, left panel). Host tissue reaction leads to degradation and dissolution of the polyglactin sutures.[28] We next wanted to examine whether the TCP-25 coating would adversely affect the degradation of the sutures in the tissue. TCP-25-coated or control sutures were subcutaneously implanted in the mice and removed after 4 days. Mechanical testing of the TCP-25-coated or control sutures recovered from the mice tissue showed no differences in the tensile strengths, suggesting that TCP-25 coating does not adversely affect the degradation of the sutures in the tissue (Figure 8b, right panel). After subcutaneous implantation, a similar loss of tensile strength was noted for both coated and control sutures compared to the sutures that were not implanted. Further, we investigated the hemolytic activity

on TCP-25-coated or control sutures. Representative SEM images showing the suture surface. Arrowhead shows bacterial biofilms formed on the suture surface. d) Bacterial LIVE/DEAD analysis showing the antibiofilm effects of the TCP-25-coated sutures. *S. aureus* and *P. aeruginosa* mature biofilms were treated with TCP-25-coated or control sutures. Staining was performed using LIVE/DEAD Baclight bacterial viability kit and followed by fluorescence microscopy. The green color shows live bacteria whereas the red color shows dead bacteria. Representative images are shown (*n* = 3). Vicryl Plus was used as a benchmark comparison. *$P \leq 0.05$, **$P \leq 0.01$, and ***$P \leq 0.001$. NS: non-significant.

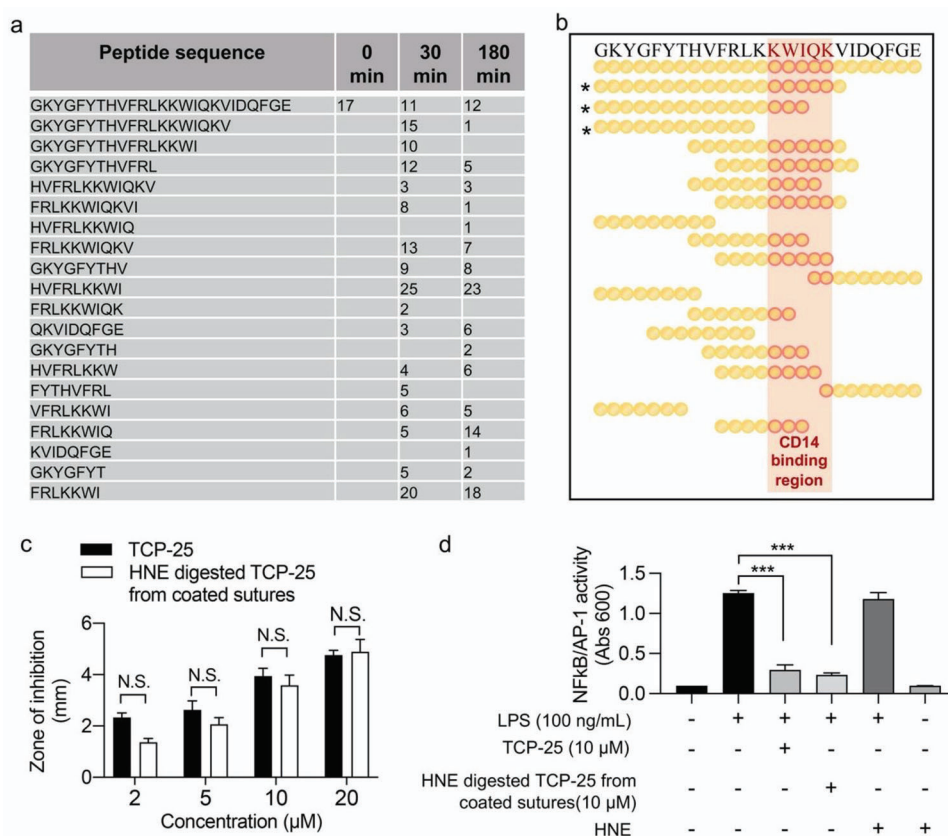| Peptide sequence	0 min	30 min	180 min
GKYGFYTHVFRLKKWIQKVIDQFGE	17	11	12
GKYGFYTHVFRLKKWIQKV		15	1
GKYGFYTHVFRLKKWI		10	
GKYGFYTHVFRL		12	5
HVFRLKKWIQKV		3	3
FRLKKWIQKVI		8	1
HVFRLKKWIQ			1
FRLKKWIQKV		13	7
GKYGFYTHV		9	8
HVFRLKKWI		25	23
FRLKKWIQK		2	
QKVIDQFGE		3	6
GKYGFYTH			2
HVFRLKKW		4	6
FYTHVFRL		5	
VFRLKKWI		6	5
FRLKKWIQ		5	14
KVIDQFGE			1
GKYGFYT		5	2
FRLKKWI		20	18

Figure 7. Human neutrophil elastase-induced TCP-25 fragmentation in TCP-25 sutures. a) Peptide fragmentation pattern of TCP-25 after treatment of TCP-25 suture with human neutrophil elastase. TCP-25 suture was incubated with human neutrophil elastase and analyzed by nano LC-MS/MS. The figure shows the sequences of main peptides and the quantity of successful identifications by mass spectrometry at 0, 30, and 180 min (*n* = 2). b) Illustration of main peptides obtained after human neutrophil elastase digestion of TCP-25 from coated sutures. *These peptides have been reported to show antibacterial effects. c) Antibacterial activity of peptide fragment products obtained after treatment of TCP-25 suture with human neutrophil elastase was analyzed by evaluating the antibacterial activity against *E. coli* by RDA. The bar chart shows quantification of the clear zone. Data are shown as the mean ± SEM (*n* = 3). d) The anti-inflammatory activity of peptide fragment products obtained after treatment of TCP-25 suture with human neutrophil elastase. NF-κB and AP-1 activation was evaluated in THP1-Xblue-CD14 reporter cells. Data are shown as the mean ± SEM (*n* = 3). ***$P \leq$ 0.001. NS: non-significant.

ADVANCED
SCIENCE NEWS

www.advancedsciencenews.com

ADVANCED
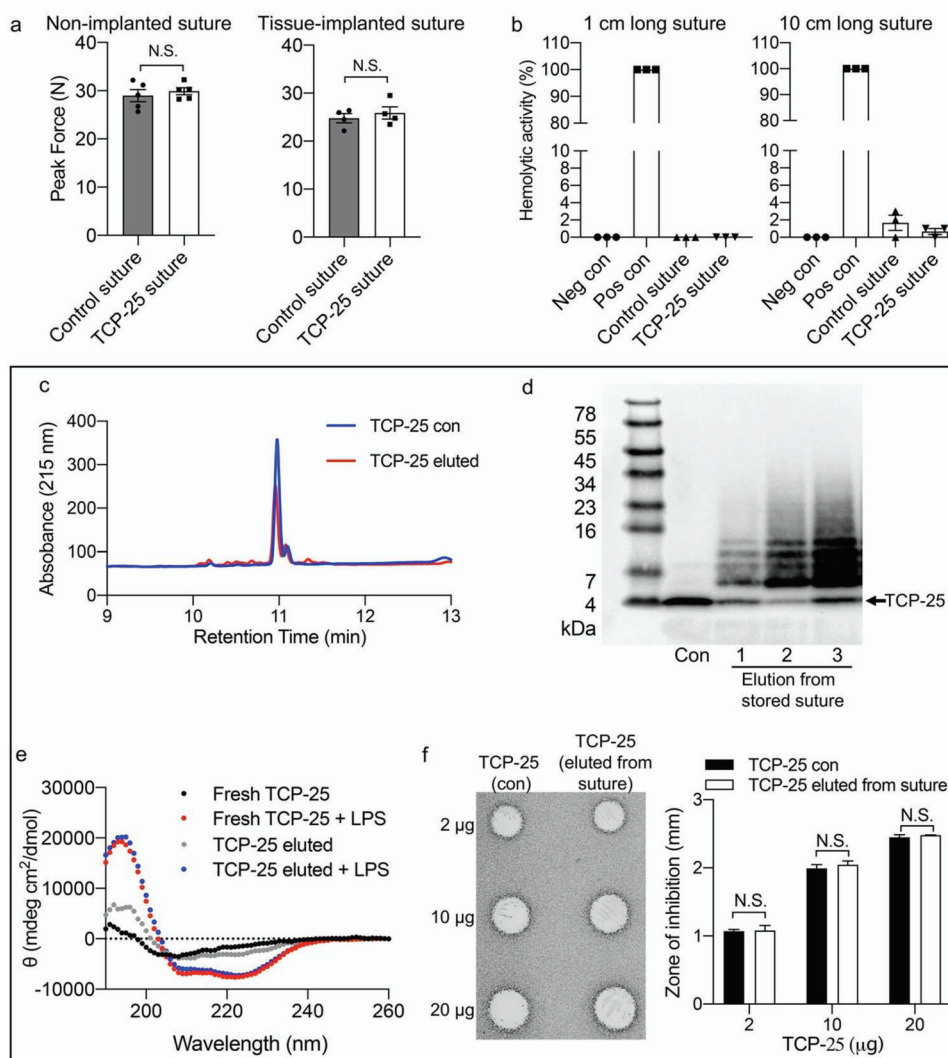**HEALTHCARE**
MATERIALS

www.advhealthmat.de

Figure 8. Determination of the tensile strength, hemolytic activity, and effects upon long-term storage of TCP-25 sutures. a) Effect of TCP-25 coating on the tensile strength of the sutures. The tensile strengths of freshly coated non-implanted (left panel) or tissue-implanted (right panel) sutures were measured. To study the effect of TCP-25 coating on the tensile strength in vivo, sutures were subcutaneously implanted in mice for 4 days. Data are shown as the mean ± SEM ($n = 5$). A Mann–Whitney U test was used to calculate *P* values. b) Hemolytic activity of control and TCP-25-coated sutures. A hemolysis assay was performed using human blood. The left bar chart shows the hemolytic activity of 1 cm long sutures, and the right bar chart shows the hemolytic activity of 10 cm long sutures (mean values ± SEM are presented, $n = 3$). NS: non-significant. c) HPLC analysis of control (fresh TCP-25) or TCP-25 eluted from coated sutures after long-term storage. TCP-25 sutures were stored at room temperature for 18 months after which peptides were eluted for HPLC analysis. d) Western blot analysis of TCP-25 eluted from coated sutures after 18 months of storage at room temperature. e) Results showing CD spectra of TCP-25 from stored sutures with and without LPS. Fresh TCP-25 was used as a control for comparison. f) Suture storage effect on the antimicrobial activity and release of TCP-25 as evaluated by radial diffusion assay using *E. coli*. Results show quantification of the clear zones. Data are shown as the mean ± SEM ($n = 3$–4). NS: non-significant.

of the TCP-25 suture. Results using a 1 or 10 cm long suture showed less than 10% hemolysis in human blood, suggesting hemocompatibility (Figure 8b).

2.9. Effects of Storage of TCP-25-Coated Suture

Further, we wanted to investigate whether the peptide was degraded upon long-term storage of TCP-25-coated sutures. TCP-25 sutures were stored at room temperature for 18 months after which the peptides were eluted for analysis. HPLC analy-

sis showed no apparent storage-related effects, and the peptide eluted from the stored TCP-25 sutures showed peaks similar to the peaks of fresh TCP-25 control peptide (Figure 8c). Non-significant storage-related effects were noticed as a few small extra peaks were observed in the chromatogram of TCP-25 eluted from stored sutures compared to freshly prepared TCP-25 control peptide. To confirm that the extra peaks in the chromatogram of eluted TCP-25 did not correspond to significant degradation of peptide, we applied Western blotting analysis. Western blotting analysis of the eluted peptide showed multiple bands of higher molecular weight confirming oligomerization (Figure 8d) of the
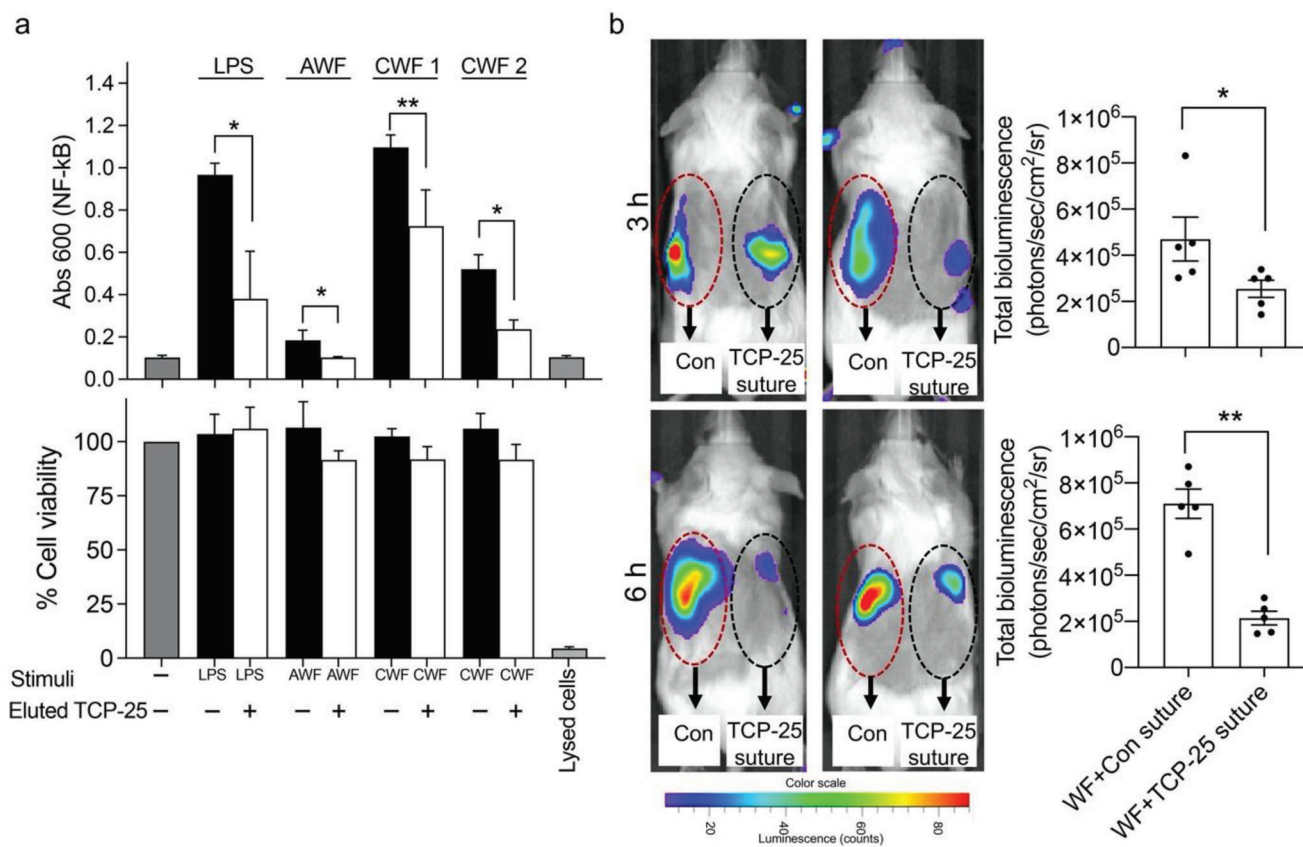
ADVANCED
SCIENCE NEWS
www.advancedsciencenews.com

ADVANCED
HEALTHCARE
MATERIALS
www.advhealthmat.de

Figure 9. TCP-25 suture targets human wound fluid-induced inflammation. a) TCP-25 suture decreases human wound fluid's pro-inflammatory ability in vitro. In a reporter assay, THP-1-XBlue-CD14 cells were used. In the presence of TCP-25 suture or control suture. cells were stimulated by acute (AWF) and chronic wound fluid (CWF) derived from infected wounds from human patients; NF-κB and AP-1 activation were evaluated by determining the production of secreted alkaline phosphatase from the reporter cells. Data are presented as the mean $\pm$ SEM ($n = 6$). P values were calculated using paired t-test. b) TCP-25 suture decreases human wound fluid's pro-inflammatory ability in vivo. TCP-25-coated sutures were contaminated with human chronic wound fluid and implanted on the back of NF-κB reporter mice. Non-invasive IVIS imaging was performed to visualize NF-κB activation. Data are shown as the mean $\pm$ SEM ($n = 5$). P values were computed using a Mann–Whitney U test. *$P \leq 0.05$ and **$P \leq 0.01$.

peptide as also reported before.[20] Next, we analyzed whether long-term storage of the TCP-25-coated suture produced any negative effect on the LPS binding capability of the TCP-25. Circular dichroism analysis showed that even after long-term storage, the peptide retained its LPS binding capacity (Figure 8e). Importantly, RDA analysis of the eluted peptide showed that no loss of antimicrobial activity upon long-term storage of TCP-25 sutures had occurred (Figure 8f). Oligomerization or aggregation of TCP-25 on suture upon storage might explain its retained bioactivity.

2.10. TCP-25 from Coated Sutures Targets Clinical Bacterial Isolates from Human Wounds and Inflammation Induced by Human Wound Fluid

After showing anti-microbial and anti-inflammatory efficacy in vitro and in animal models, we finally explored whether TCP-25-coated sutures could also target clinical bacterial isolates from wounds and inflammation pertaining to human wounds. When incubated with various clinically derived human wound isolates, clear zones of inhibition were observed around the TCP-25-coated suture (Figure S9, Supporting Information). Further,

acute wound fluid (AWF) and chronic wound fluids (CWF) derived from patients with wounds colonized by bacteria such as *S. aureus* and *P. aeruginosa* were used to activate inflammation in THP-1 reporter cells. TCP-25 eluted from the coated suture caused a reduction in the human wound fluid-induced inflammation in THP-1 cells (**Figure 9**a, upper panel). Results from the MTT assay showed that TCP-25 at these concentrations was not toxic to the cells (Figure 9a, lower panel). Finally, in an in vivo setting, TCP-25-coated sutures were contaminated with human chronic wound fluid and implanted on the back of NF-κB reporter mice. Non-invasive IVIS imaging was performed to visualize NF-κB activation. Control sutures contaminated with human chronic wound fluid induced significantly more inflammation than the TCP-25-coated sutures (Figure 9b). Altogether, results suggest that TCP-25-coated sutures have the potential to reduce infection and inflammation in a complex human wounding situation.

3. Conclusion

Using a combination of in silico molecular modeling studies, in vitro antimicrobial, biochemical, and biophysical assays

ADVANCED
SCIENCE NEWS
www.advancedsciencenews.com

ADVANCED
HEALTHCARE
MATERIALS
www.advhealthmat.de

combined with in vivo models, we here show a proof-of-concept demonstrating the possibility of functionalizing a polyglactin suture material with a dual action host defense peptide that can target both bacteria and the excessive inflammatory response. This broad capability may be of biological and clinical importance. In the initial contact with tissues, it is plausible that a given biomaterial also induces an immune response per se, which may cause dysregulation of inflammatory responses, leading to inefficient host defense and causing a given biomaterial to become infection-prone.[29] Moreover, in the case of bacterial adhesion, the release of bacterial products, such as lipoteichoic acid (LTA) and LPS, may stimulate inflammation in the vicinity of biomaterials. The possible mechanisms underlying suture-associated infections have only been partially explained, mainly with research focused on bacterial adhesion and biofilm formation. Though, applying the above reasoning to sutures, it is plausible that creating a local suture environment that counteracts bacteria but controls immune responses could be a new attractive strategy for optimizing and boosting infection control. Another serious problem is the declining effectiveness of antibiotics and other antimicrobials due to antimicrobial resistance (AMR) development. The development of resistance is particularly important in surgical procedures in which the combination of extensive antibiotic use, high risk of systemic spread, and bacterial sepsis leads to a high frequency of infections for which "last resort" antibiotics need to be used. Considering the above issues, an unmet need for new biologically-oriented strategies exists that is based on the multi-pronged action of TCP-25 which targets bacteria in a new way; hence, minimizing resistance problems and also controlling the excessive inflammatory process.

At present, multiple antimicrobials are in use or under development for use on sutures.[30] Based on its wide use, we therefore decided to use triclosan as a benchmark antimicrobial in the studies.[31] As mentioned in the Introduction, increasing concerns with the use of this antiseptic exist. Thus, triclosan resistance is frequently reported in *S. aureus*.[32] Moreover, Nadafpour et al.[33] studied the bacterial colonization on various suture materials used in oral implantology. Vicryl Plus sutures showed the highest buildup of *E. coli* and *S. aureus* when compared with Vicryl alone, and triclosan-coated Vicryl Plus sutures exhibited no benefit over the commonly used silk sutures in terms of causing a decrease in the number of bacteria. Elsolh et al. performed a meta-analysis[34] to determine if antibiotic-impregnated sutures, including triclosan, could prevent post-operative surgical site infections and complications in abdominal surgery. No evidence was found by them to support routine use of these sutures. Recently, a systematic review and meta-analysis of randomized controlled trials[35] showed no benefits from the use of triclosan-coated sutures. The authors state that global and national guidance should be reevaluated for the recommendations for routine use of triclosan-coated sutures. In this context, it should be mentioned that in 2016, the United States Food and Drug Administration (FDA) banned the triclosan incorporation in household products; and then, prohibited triclosan usage in over-the-counter antiseptic products without premarket review.[36] The European Commission, in 2016, did not approve triclosan as an active substance for use in biocidal products for product-type 1.[37] Given the questionable risk-benefit of triclosan, multiple other antimicrobial sutures are in use or under development.[30] These sutures incorporate, among others, classical antiseptic products, such as chlorhexidine, polyhexamethylene biguanide (PHMB), octenidine, and povidone–iodine. Other substances used are derived from natural products, such as chitosan, aloe vera, silver nanoparticles, or different antibiotics. Notably, octenidine and chlorhexidine have been applied on Vicryl by dip coating as also used in this study.

In contrast to the above-mentioned antimicrobials, the present work adds a previously unexplored pharmacological functionality to Vicryl sutures that is based on the capability of TCP-25 not only to kill bacteria but also to scavenge multiple bacterial products and concurrently inhibiting downstream CD14/TLR-mediated inflammatory responses.[16] In this context, it is notable that the findings of our study highlight the specific interaction between TCP-25 and Vicryl suture fibers. Through the utilization of QCM-D, we demonstrated peptide binding and affinity to the suture fibers, which was further substantiated by molecular modeling and simulations using a coarse-grained model of TCP-25 and polyglactin 910 copolymer. Moreover, O-PTIR spectroscopy measurements confirmed the presence of TCP-25 on the fibrillar surface of coated sutures, and fluorescence imaging demonstrated intense distribution of TCP-25 on the surface and between Vicryl fibrils. Taken together, these findings provide a comprehensive characterization of the TCP-25-polyglactin interaction supporting the in vitro and in vivo data.

Clearly, it remains to be investigated whether such bioactive TCP-25 functionalized sutures can prevent SSIs in the clinical setting. It should; however, be mentioned that the dual action concept based on TCP-25 has already shown promise in the setting of wound healing and infections,[17,18] and that a TCP-25 hydrogel is currently in clinical development, undergoing phase I safety studies on humans.[38] By utilizing a clinically approved absorbable suture and a peptide with established safety profiles, our study therefore paves the way for the expedited clinical translation of TCP-25-coated Vicryl sutures, addressing the urgent need for effective coated biomaterials that combat infections and inflammation in surgical settings. Moving forward, future development of the final suture product should include further evaluation and standardization of the coating procedure, suture hydrolysis and peptide stability determination, analysis of optimal peptide release kinetics, assessment of biocompatibility, and comprehensive preclinical and clinical studies.

4. Experimental Section

Materials: TCP-25 (GKYGFYTHVFRLKKWIQKVIDQFGE) peptide was synthesized by Ambiopharm (Spain). The tetramethylrhodamine (TAMRA)-labeled TCP-25 was synthesized by Biopeptide Co (San Diego, CA, USA). The purity of the peptide was 95% as confirmed by mass spectral analysis (MALDI-ToF Voyager).

Microorganisms: Bacterial strains used included *E. coli* (ATCC 25922), *P. aeruginosa* PAO1, and *S. aureus* (ATCC 29213). Bioluminescent *P. aeruginosa* Xen41 (PerkinElmer, Akron, OH) and *S. aureus* SAP229 were used for experiments requiring infection imaging. In some experiments, clinical isolates of *S. aureus* (2404, 2278, 2405, 2528, 1779), *P. aeruginosa* (27.1, 23.1, 13.2, 10.5, 62.1), *S. epidermidis* (2282), and *E. faecalis* (2374) were also used. These isolates were obtained either from skin or wound infections at the Department of Bacteriology, University Hospital, Lund, Sweden.

Preparation of TCP-25-Coated Suture: A Vicryl suture (3-0, ETHICON, Johnson & Johnson International, Belgium) was cut into 10 cm pieces.

A 2% TCP-25 solution was prepared by solubilizing the peptide in sterile water. The suture pieces were coated in TCP-25 solution (5 mL) on a shaker for 1 h at room temperature. After coating, the sutures were air-dried in a class II biosafety cabinet at room temperature (20 °C $\pm$ 1 °C) for 1 h. Control sutures were coated with only sterile water.

To examine the effects of TCP-25 coating concentration on antibacterial properties, sutures were coated with 0.1%, 0.5%, 2.0%, or 4.0% TCP-25 solution for 2 h. To examine the effects of coating time on antibacterial properties, sutures were coated with 2% TCP-25 solution for 1, 2, 4, 8, and 24 h at room temperature. To examine the effects of coating temperature on antibacterial properties, sutures were coated with 2% TCP-25 solution at 21 °C, 37 °C, or 50 °C for 2 h. Coated sutures were kept at -80 °C in moisture-free conditions until further use. To elute peptide, coated sutures were added in Tris (10 mM, pH 7.4) on a shaker for 30 min at room temperature. Eluted solutions were stored at -80 °C. Suture TCP-25 loading was determined as described previously.[39] Briefly, sutures were weighed before and after coating with TCP-25. Drug loading was calculated using the following equation.

$$\text{Drug loading (\%)} = ((\text{Weight after coating} - \text{weight before coating}) / \text{weight before coating}) \times 100 \quad (1)$$

Protein Estimation: For the estimation of protein concentration, Nanodrop method (ND 1000, Thermo Scientific) was used at 280 nm using TCP-25 extinction coefficient (8 480 M^{-1} cm^{-1}) and molecular weight (3088,62 Da).

Radial Diffusion Assay (RDA): Ten mL of tryptic soy broth (TSB) form was used to grow *E. coli* to the mid-logarithmic phase. Afterward, the bacteria were washed in 10 mM Tris (pH 7.4). Bacteria (4×10^6 CFU) were added to 15 mL of the underlay agarose gel comprising 0.03% w/v TSB, 1% w/v low electro endosmosis type (EEO) agarose (Sigma, St Louis MO, USA), and 0.02% v/v Tween 20 (Sigma). Underlay gel was added to a 144 mm diameter petri dish. Once the gel became solid, using a biopsy punch, 4 mm-diameter wells were cut into the underlay gel. A sample containing 6 µL of the test sample (solution eluted from the sutures) was added to each well. Afterward, plates were incubated at 37 °C for 3 h, and 15 mL of overlay gel (6% TSB and 1% low-EEO agarose in distilled H_2O) was added to cover underlay gel. The plates were incubated at 37 °C for 18 h. The antimicrobial activity was determined as a clear zone-to-well diameter (excluding the 4 mm well).

SDS-PAGE: To study the effects of storage of TCP-25-coated suture, sodium dodecyl sulfate-polyacrylamide gel electrophoresis (SDS-PAGE) was employed to study eluted peptide. Briefly, the sample (5 µL) was loaded on a 10–20% Tris–Tricine gel and run for 90 min at 100 V. Two micrograms of TCP-25 solubilized in 10 mM Tris (pH 7.4) was used as control. Coomassie Brilliant blue (Invitrogen, Rockford, IL, USA) was used to stain the gel.

Western Blotting: Immediately following electrophoresis, western blotting was performed as described before.[16]

Peptide Release Assay: For the peptide in vitro release assay with some modifications, a wound scenario was simulated. A Transwell insert system (VWR Tissue Culture Plate Insert – 6 well, 0.4 µm pore size, VWR International) was used in combination with a six-well plate. Twenty 3 cm long pieces of TCP-25-coated sutures were placed on porous filter in the apical compartment. Two mL of elution buffer (10 mM Tris, pH 7.4) was added to the basolateral compartment. The elution buffer stayed in contact with the porous filter; and thus, with the sutures (as illustrated in Figure 1d). The plate was covered and sealed with parafilm to prevent evaporation of the solution. The plate was kept at 37 °C on a shaker at 60 rpm. A 20 µL sample was taken from the basolateral part at the designated times and instantaneously replaced with 20 µL of new Tris buffer. A spectrophotometer (Nanodrop, Thermofisher) was employed to measure absorbance at 280 nm (A_{280}). The results were represented as cumulative TCP-25 release (mg mL^{-1}).

Scanning Electron Microscopy (SEM): Briefly, the bacteria were incubated for 15 min at 37 °C with coated and uncoated sutures after which they were transferred to new tubes. Sutures were washed two times in 0.1 M Sorensen's phosphate buffer (pH 7.4). The samples were further processed for SEM as described previously.[18] For SEM of sutures with biofilm, after 48 h of microtiter plate incubation and suture removal (as described in the biofilm section), the sutures were washed in Sorensen's buffer and processed for SEM as mentioned above.

Quartz Crystal Microbalance With Dissipation Monitoring (QCM-D): QCM-D measurements were performed using a QSense E4 system from Biolin Scientific (Gothenburg, Sweden) with four standard flow modules (QSense, Biolin Scientific), each equipped with silicon dioxide surfaces (QSense, Biolin Scientific, QSX 303 SiO_2, 4.95 $\pm$ 0.05 MHz, 14 mm diameter, 0.3 mm thickness, and 17.7 ng cm^{-2} mass sensitivity). Prior to use, cells, tubings and o-rings were thoroughly cleaned with a 2% Hellmanex solution and multiple Milli-Q (MQ) water rinses, combined with bath sonication, followed by rinsing in pure ethanol and subsequent drying by N_2 flow. The SiO_2 surfaces were sequentially washed in 2% Hellmanex, MQ water, and ethanol; then, dried with N_2, and plasma cleaned (Model PDC-32G, Harrick Plasma, USA) in residual air for 5 min. Right after, the SiO_2 surfaces were incubated in a 0.1% w/w Poly-L-lysine (MW 150–300 kDa, Sigma–Aldrich, Merck, New Jersey, USA) solution in MQ water (pH 9.5) for 30 min at room temperature. After that, SiO_2 surfaces were thoroughly rinsed with MQ water and dried with nitrogen. One hundred mg of finely cut fiber (50–100 µm length) in 1 mL ethanol was subsequently deposited on poly-L-lysine-functionalized SiO_2 surfaces and left incubating overnight at room temperature. This led to solvent evaporation and subsequent fiber immobilization onto the positively charged poly-L-lysine-functionalized surfaces. Finally, fiber-functionalized surfaces were thoroughly rinsed in MQ water and mounted in QCM-D measurement cells. After reaching a stable baseline of frequency (ΔF) and dissipation (ΔD) shifts under 0.1 mL min^{-1} MQ water flow (controlled through a peristaltic pump), a 0.001% w/w peptide solution in MQ water was injected into the measurement chamber at 0.1 mL min^{-1} flow rate. Peptide adsorption onto fiber-functionalized sensors was confirmed by frequency changes (ΔF) of -100 ± 27 Hz and dissipation changes (ΔD) of ($+42 \pm 11) \times 10^{-6}$, with respect to pure MQ water. This was followed by rinsing with MQ water in the absence of peptide. The possible adsorption of the peptide onto the underlying poly-L-lysine surface was ruled out with a control experiment, in which the interaction of peptide with fiber-free Poly-L-lysine-functionalized SiO_2 surfaces was monitored under the same experimental conditions. Measurements were performed at room temperature.

In Silico Modeling and Simulations of Vicryl With TCP-25 (Coarse-Grained Parameterization of Vicryl): A coarse-grained (CG) model of Vicryl polymer was developed using the Martini 2.2 forcefield.[40] Vicryl or polyglactin 910 is a copolymer made of 90% glycolide and 10% lactide. The molecular weight is $\approx$80 kDa, which translates to $\approx$600-mer.[41] To simplify the system, an atomic model of a 10-mer polyglactin containing 9 subunits of glycolide and 1 subunit of lactide was first built using the CHARMM-GUI Polymer Builder[42] and the CHARMM36m all-atom forcefield.[43] The polymer was solvated in a box of TIP3P water molecules and neutralized with 0.15 M NaCl salt. Then, energy minimization and equilibration were performed following the CHARMM-GUI standard protocol.[44] A 1 µs production simulation was performed at 310 K and 1 atm using temperature coupling to Nosé–Hoover thermostat[45] and isotropic pressure coupling to Parrinello–Rahman barostat.[46] The electrostatic interactions were computed using the particle mesh Ewald (PME) method,[47] while the van der Waals interactions were cut off at 1.2 nm with a force-switch smoothing function applied between 1.0 and 1.2 nm. A simulation time-step of 2-fs was used.

To generate the equivalent model for polyglactin in the CG Martini forcefield, the mapping scheme derived in a previous study was initially followed.[48] Each glycolide and lactide subunit was mapped into one bead and represented by the Na bead type (Figure S3a, supporting Information). Unlike the previous study, the polyglactin model had a negatively charged carboxyl group at one end of the polymer and a hydroxyl group at the other end. The former was mapped into two small beads of types SQa and SNa, while the latter was mapped into one bead of type P3. The resultant CG model of polyglactin was then solvated with Martini water molecules and neutralized with 0.15 M NaCl salt. Energy minimization

was performed using the steepest descent method and a short 100 ps equilibration simulation was conducted. Then, a 1 µs production simulation was conducted using a 10-fs time step. The electrostatic interactions were computed using the reaction field method with a 1.1 nm cut-off, while the van der Waals interactions were cut off at 1.1 nm with a potential shift Verlet scheme. Temperature and pressure was maintained at 310 K and 1 atm by a velocity rescaling thermostat[49] and an isotropic coupling to a Parrinello–Rahman barostat, respectively. The distribution of bonds, angles, and dihedrals from the CG simulation was then compared to the all-atom simulation (Figure S3b–d, Supporting Information). The bonded parameters were iteratively modified to match the distribution of the all-atom simulation.

The final model was multiplied to generate 50-mer and 100-mer polyglactin polymers with the same 9:1 ratio of glycolide:lactide. These longer polymers were subject to a similar protocol of energy minimization, equilibration, and a 1 µs production run described above. The structure of the polymers at the end of these simulations was then used for a self-assembly simulation to build a large Vicryl polymer aggregate. Thus, 50 copies of the polyglactin polymers were solvated with Martini water molecules, and the system was neutralized with 0.15 M NaCl salt. The systems were subject to the same energy minimization and equilibration protocols. A 1 µs simulation was then performed at 320 K using parameters described above to allow the polymer to self-aggregate. The structure of the polymer aggregates was then extracted from these simulations for subsequent simulations with TCP-25.

Coarse-Grained Simulation of Vicryl With TCP-25: The NMR structure of HVF18 (PBD: 5Z5X)[16] was used as a template to model the TCP-25 peptide. The missing N-terminal residues (GKYGFYT) were built using Modeller version 9.21,[50] and the model with the lowest discrete optimized protein energy was chosen. The TCP-25 model was converted to CG representation using the Martini 2.2 forcefield with the standard ElNeDYn elastic network model to preserve the secondary structure.[51] Ten copies of TCP-25 peptide were added into a box containing the Vicryl polymer aggregate made of 100-mer polyglactin generated in the previous step (Figure 2a). The TCP-25 peptides were placed at least 2 nm away from the surface of the polymer and from each other. The system was then solvated with Martini water molecules and neutralized with 0.15 M NaCl. Energy minimization was performed using the steepest descent method. A 100 ns equilibration simulation was conducted whereby positional restraints with force constants of 500 kJ mol^{-1} nm^{-2} were applied to every bead of the polymer, and 1000 kJ mol^{-1} nm^{-2} was applied to every backbone bead of the peptide. Three independent 10 µs production simulations were then performed with different initial velocities. The temperature was maintained at 320 K using the velocity rescaling thermostat,[49] and the pressure was maintained at 1 atm using an isotropic pressure coupling to a Parrinello–Rahman barostat.[46] The electrostatic interactions were calculated using the reaction field protocol with a 1.1 nm distance cut-off, while the van der Waals interactions were truncated at 1.1 nm with a potential shift Verlet scheme. A 10-fs integration time step was used. Using the same protocols, similar simulations were performed for a system with a higher concentration of TCP-25 peptides (20 copies), a shorter chain of polyglactin (50-mer), and lower temperatures (310 and 298 K). All simulations were performed using GROMACS 2022[52] and visualized using VMD.[53]

Optical Photothermal Infrared Microspectroscopy: Optical photothermal infrared microspectroscopy (O-PTIR) is an analytical technique based on the photothermal effect induced by scanning infrared laser measured by scattered probe light.[54] O-PTIR was performed at the SMIS beamline, SOLEIL synchrotron (France). Sutures were deposited directly on the glass slide and used for measurements. The photothermal effect was detected by modulating the CW 532 nm laser intensity induced by an infrared laser. The IR source was a pulsed, tuneable quantum cascade laser, set to to 22% of laser intensity, scanning from 1800 to 1300 cm^{-1}, at an 80-kHz repetition rate. Further details about the fundamentals of the technique and the instrument itself can be found in a previous work.[55]

Cryosectioning: To facilitate fluorescence imaging of TCP-25, Vicryl sutures (3-0, ETHICON, Johnson & Johnson International, Belgium) were coated as described before (see 'Preparation of TCP-25-Coated Suture'

in The Experimental Section), except that TCP-25 (spiked with 5% TCP-25-Cy3) was used for the coating. Coated sutures were then mounted in OCT compound for cryosectioning. Suture cryosections (8 µm thick) were prepared using a cryostat (Leica Biosystems). Slides were washed in PBS (5 min, RT), dried, and mounted with antifade mounting medium (PermaFluor, ThermoFisher Scientific). The sections were then imaged using fluorescence microscopy (AxioScope.A1, Carl Zeiss, Germany).

High-Performance Liquid Chromatography: One or 2 µg of TCP-25 eluted from the suture was analyzed by reverse-phase high performance liquid chromatography (HPLC), as reported by Petruk et al.[20] Two micrograms of TCP-25 freshly dissolved in 10 mM Tris at pH 7.4 was used as a control. Samples from three different elutions were analyzed.

Analysis of Intrinsic Fluorescence: The binding of LPS to TCP-25 was analyzed by determining the intrinsic fluorescence of the peptide as reported previously.[18] Ten µM TCP-25 eluted from the suture was titrated with increasing LPS concentrations (2–100 µg mL^{-1}). Kd was computed using GraphPad Prism v9 assuming a single binding site.

Circular Dichroism (CD) Spectroscopy: The secondary structure of TCP-25 eluted from suture was evaluated by Jasco J-810 spectropolarimeter (Jasco, USA). The spectropolarimeter had a Jasco CDF-426S Peltier set to 25 °C. The cell path length was 0.2 cm. The spectrum was acquired between 190 and 260 nm (20 nm min^{-1} scan speed). TCP-25 (10 µM, 200 uL) alone or with 100 µg mL^{-1} LPS was used for the experiment. Acquired spectra were corrected for buffer contribution with or without LPS and converted to mean residue ellipticity, θ (mdeg cm^2 dmol^{-1}). Content of α-helical structure was calculated as reported previously.[56] The experiment was performed three times using a new elution of TCP-25 each time.

Viable-Count Assay: Viable-count assay was performed as reported previously.[18] Briefly, bacteria were incubated at 37 °C for 5 min and 1 and 2 h with sutures coated in TCP-25 or control sutures under various conditions. Buffers used in this assay were 10 mM Tris with 5 mM glucose, pH 7.4, and 10 mM Tris with 1.3% glycerol, pH 7.4 supplemented with 20% human plasma or 20% acute wound fluid. Samples obtained after serial dilutions were plated on TH broth agar and kept overnight in an incubator at 37 °C.

Antibacterial Effects of TCP-25 Suture on Bioluminescent Bacteria: Bioluminescent bacteria were grown in TH medium until OD 0.4. Bacteria were then washed in 10 mM Tris pH 7.4 and suspended in 10 mM Tris with 5 mM glucose, pH 7.4, or 10 mM Tris with 1.3% glycerol. The bacterial suspension (10^7 CFU in 200 mL) and 1 cm long TCP-25-coated or control sutures were placed in a white polystyrene 96-well plate. The plate was kept at 37 °C in an incubator. The bioluminescent signals were longitudinally imaged by IVIS (PerkinElmer, USA) and quantified by a luminometer.

Live–Dead assay: Live–dead bacterial staining was performed as described previously.[17] Briefly, a 1 cm long piece of TCP-25-coated or control suture was added to 200 µL *P. aeruginosa* (PAO1) or *S. aureus* (ATCC 29213) suspension and incubated for 30 min at 37 °C. Fifty µL of mixture of components A and B was added to the samples; and then, incubated at room temperature for 15 min in the dark. Suture pieces were taken out of the stained suspension, placed on a slide, and analyzed by fluorescence microscopy.

NF-κB/AP-1 Assay: THP1-Xblue TM – CD14 reporter cells (InvivoGen, San Diego, USA) were used to study nuclear factor kappa beta/activate protein (NF-κB/AP-1) activation. Assay was performed as reported previously.[18] Briefly, 180 µL of 1 × 10^6 cells was seeded into 96-well plates and treated with 10 µL TCP-25 eluted form suture, with LPS (from *E. coli* O111:B4, Sigma–Aldrich), or with 5 µL of human wound fluid. After incubation for 20 h at 37 °C in 5% CO$_2$, 20 µL of media from each well was moved in a new 96-well plate having 180 µL QUANTI-Blue reagent (InvivoGen). Plates were then incubated at 37 °C for 1–2 h. The amount of secreted embryonic alkaline phosphatase (SEAP) was measured at OD 600 nm.

Cell Viability Assay: The viability of THP-1 cells from the abovementioned assay was assessed as described previously.[18]

Cytokine Assay: Mice from suture-induced inflammation model were euthanized 24 h after suture implantation. Implanted sutures were recovered from the mouse and added to a pre-chilled Eppendorf tube. Fifty microliters of Tris buffer was added to the suture and vortexed for 10 min for elution. Finally, the tube was centrifuged (2000 × *g* at 4 °C, 5 min), and

the supernatant was collected for cytokine analysis. Tumor necrosis factor alpha and interleukin 6 (TNF-α and IL-6, respectively) were assessed using the Mouse Inflammation Kit (Becton Dickinson AB, Franklin Lakes, NJ) as described by the manufacturer.

Hemolytic Activity: Fresh venous blood was collected from healthy donors in lepirudin tubes (50 µg mL^{-1}). One or 10 cm of suture coated with TCP-25 was placed in tubes containing 0.5 or 1 mL, respectively, of 25% of human blood diluted with RPMI-1640- GlutaMAX-I without phenol red (Gibco). The hemolytic activity of only the suture was analyzed by putting 1 or 10 cm suture coated with only buffer. Blood (25%) in RPMI was used as a negative control. The positive control was obtained by mixing 75 µL of blood solution with 225 µL 5% Tween-20 in RPMI-1640-GlutaMAX-I without phenol red. Samples were incubated for 1 h at 37 °C (5% CO$_2$) and tubes were centrifuged at 800 × g. One hundred µL of each sample was transferred to a flat-bottom 96-wells plate, and absorbance was measured at 450 nm. The percentage of hemolysis was calculated as reported previously.[18]

In Vivo Peptide Release in Mice: SKH-1 hairless 10–12-week-old male mice were used for the TCP-25 in vivo release study. Mice were anesthetized using 4% isoflurane (Baxter). All procedures were performed under aseptic conditions. Sutures coated with TAMRA-labeled TCP-25 were used for fluorescence bioimaging. With the help of a needle, a 2 cm piece was subcutaneously implanted into the back of hairless SKH-1 mice. TCP-25 release was longitudinally observed by acquiring fluorescence intensity using an IVIS imaging system (Perkin Elmer). Data were analyzed with Living Image 4.0 Software (PerkinElmer).

Experimental Mouse Model of Suture Infection: SKH-1 hairless mice (8–10 weeks old females) were used for the experimental model of suture infection. Anesthesia was achieved using a mixture of isoflurane (Baxter) for induction (4%) and maintenance (2%). All procedures were performed under aseptic conditions. The dorsum of the mouse was cleaned with an ethanol wipe and wiped with sterile gauze. A 5 mm incision was made on the dorsum's skin, and the tip of the scissors was used to make a small pocket. A 2 cm long piece of TCP-25 suture or control suture was deposited in the pocket with the help of a needle on each side of the dorsum. With the help of a pipette, in the pocket, sutures were contaminated with bioluminescent *S. aureus* (SAP229) or *E. coli* (ATCC 25922) (10^5 CFUs in 20 µL Tris buffer). The incision was closed with the help of tissue glue.

In some experiments, in addition to the bacterial visualization, to monitor the tissue distribution of TCP-25, sutures coated with TAMRA-labeled TCP-25 were used followed by IVIS imaging in both bioluminescence (for bacteria) and fluorescence (for TCP-25) modes.

NF-κB Reporter Mouse Model of Suture-Induced Inflammation: BALB/c tg(NF$\kappa\beta$-RE-Luc)-Xen reporter mice (Taconic Biosciences, Albany, NY, USA) were used to evaluate the anti-inflammatory effects of TCP-25-coated sutures. Male mice (8–10 weeks old) were used in this study. As described above for the suture infection model, under aseptic conditions, a 5 mm incision was created on the skin of the mouse's dorsum, and a small pocket was made. A 2 cm long piece of TCP-25 suture or control suture was deposited in the pocket with the help of a needle on each side of the dorsum. Using a pipette, in the pocket, sutures were contaminated with 2 µg LPS (in 20 µL Tris buffer). The incision was closed with the help of tissue glue. For inflammation analysis, longitudinal in vivo imaging with IVIS was employed to determine NF-κB activation. One hundred µL of D-luciferin (PerkinElmer, 150 mg kg^{-1} body weight) was intraperitoneally injected 15 min before IVIS imaging. Bioluminescence was quantified using Living Image 4.0 Software (PerkinElmer). In the experiment where TCP-25-coated sutures were contaminated with human chronic wound fluid, the abovementioned procedures were followed except that instead of LPS, 10 µL of wound fluid was used to contaminate sutures in the subcutaneous pocket.

Nano LC–MS/MS Analysis: For peptide digestion, 1 cm long piece of TCP-25-coated suture was incubated with HNE (0.1 µg, in 20 µL 10 mM Tris, pH 7.4) at 37 °C for 30 min and 3 h. HNE-digested TCP-25 peptides were separated with nanoflow reversed-phase chromatography using an Evosep One liquid chromatography (LC) system (Evosep) after loading the samples on Evosep tips. Separation was performed with the 60 SPD method (gradient length 21 min) employing an Evosep column (8 cm × 150 µm) packed with ReproSil-Pur C18-AQ particles (1.5 µm). The Evosep One system was coupled to a capacitive source mounted on a timsTOF Pro mass spectrometer (Bruker Daltonics). The mode used to run the instrument was DDA PASEF mode. The raw files were searched against the Human Uniprot database (release 2021-03-09) using PEAKS Pro version with the following settings, MS tolerance 30 ppm, MSMS 0.02 Da, no enzyme, oxidation of methionine (variable), and maximum one post-translational modification per peptide.

Biofilm Studies: To study the antibiofilm activity of TCP-25-coated sutures, biofilms of *S. aureus* (ATCC 29213) and *P. aeruginosa* PAO1 were used. To study the direct effect of TCP-25 suture on mature biofilms, *S. aureus* biofilms were grown on 96-well round-bottomed vinyl flexible plates (Corning, Kennebunk, USA). Growth media (100 µL), 0.5% Tryptic soy broth, and TBS, supplemented with 0.2% glucose, were added to each well. Five µL of 1 × 10^8 CFU mL^{-1} bacteria was added to the growth medium. Similarly, *P. aeruginosa* were grown in M63 growth medium supplemented with 0.5% casamino acids, 0.2% glucose, and 1 mM MgSO$_4$, on the flat bottom 96 well microplates (Greiner Bio-One, Frickenhausen, Germany). For both bacterial strains, 5 µL of 1 × 10^8 CFU mL^{-1} bacteria was added to the growth medium. After bacterial addition, plates were sealed with microplate seals and placed in moist containers to prevent evaporation. The containers were then incubated at 37 °C undisturbed for 48 h to achieve mature biofilms. The mature biofilm in the well was washed (100 µL of Tris) twice to remove planktonic cells, after which an additional hundred µL of Tris was added to the well. For treatment of the biofilm, 1 cm long pieces of TCP-25 suture or control suture were then added to the wells. The plate was sealed, placed in the moist container, and incubated at 37 °C for an additional 2 h. After treatment, to count viable bacteria, biofilm was disrupted by scraping using a pipette tip. A 10 µL aliquot was then removed from each well, serially diluted, and plated for CFU determination. For visualization of the treatment effects on biofilm-associated bacteria, biofilms were removed from the wells by scraping and stained with the Live/Dead bacterial viability Kit (ThermoFischer Scientific). Mixture of component A and B (0.3 µL each) was added to the biofilm samples and mixed. Samples were incubated in the dark (15 min, room temperature), and 10 µL was placed on a glass slide and viewed by fluorescence microscopy.

To evaluate the impact of TCP-25 suture on biofilm growth in the microtiter plate and on the suture itself, 30 min after the addition of bacteria in the growth medium for biofilm formation, a 1 cm piece of TCP-25 suture was added to the bottom of the well. As mentioned above, this was followed by incubation (37 °C, 48 h). Suture pieces were removed after incubation, and wells were washed (100 µL of Tris) twice to remove planktonic cells. Extracted suture pieces were processed further for staining with the Live/Dead bacterial viability kit, viable count for CFU determination, or SEM. CFU counts of the suture-associated biofilm were conducted by placing the suture into tubes containing 100 µL of Tris buffer. Samples were then sonicated (1 min × three times) to disrupt the biofilm. Samples were taken and processed according to the previously mentioned procedure for viable count assay. For the Live/Dead analysis, the above-mentioned protocol was used with the modification of the sutures being placed into the premixed stain to avoid disruption of the biofilm by vortexing.

To assess the biomass of the wells, the plate was further processed by washing each well twice with distilled water before adding 150 µL of 1% crystal violet. The plate was incubated for 15 min, after which, the wells again were rinsed in distilled water. 200 µL of 96% ethanol was then added to the wells for an additional 15 min before 120 µL from each well was transferred to a fresh microtiter plate and analyzed at OD$_{600}$ to determine the absorbance in the wells.

Tensile Strength Determination: The tensile strength of the sutures was analyzed using Instron 8511.20 (Instron Corp). Ten cm long suture pieces were mounted on the sample holder by turning the thread around a cylindrical bolt three times followed by three single knots to secure the suture. The same process was repeated on both ends of the testing jig, and the instrument was moved using a hydraulic controller to ensure that no relaxation had occurred in the string, and at the same time, care was taken to not load the threads to a force of > 1 N. The distance from the center of the cylindrical bolts was measured using a Vernier caliper and assigned as L0 or the original length. The samples were then axially pulled at a predefined

ramp speed of 0.25 mm^{-1} s, and the failure force and displacement (L1) were recorded digitally using a 250 N load cell. Maximum force at breaking was obtained from the force versus displacement data. Further, % elongation was calculated using the formula: %Elongation = $(L1-L0)/L0 \times 100$, where $L1$ = displacement at failure and $L0$ = original length of the thread before the test was started (measured as the distance between the center of the holding bolts). Data acquisition was done with MTS FlexTest 40 Controller, MTS TestSuite Multipurpose Elite Software.

Wound Fluid From Patients: Wound fluids from chronic venous leg ulcers and acute wounds were used in this study and the collection method had been described previously.[57] Wound fluids used for the experiments were collected from patients with positive *P. aeruginosa* and *S. aureus* cultures. Briefly, using a tabletop centrifuge, wound fluids were centrifuged at 10 000 rpm. Aliquots were prepared and stored at $-20\ ^\circ$C until further used.

Data Analyses: For normally distributed data, Student's *t*-test was used to determine differences in the mean between two groups, and Mann–Whitney test was used otherwise. For more than two groups, means were compared using a one-way ANOVA with post hoc (Tukey) for normally distributed data or Kruskal–Wallis test otherwise. Data are presented as means ± SEM. Individual figure legend includes details of statistical analysis used for the experiment. Data analysis was accomplished by using GraphPad Prism software v8. *P* values < 0.05 were considered to be statistically significant.

Ethics Statement: Experiments included in this study were accomplished according to Swedish Animal Welfare Act SFS 1988:534. Approval was obtained from the Animal Ethics Committee of Malmö/Lund, Sweden (permit numbers M252-11, M131-16, M88-91/14, M5934-19, 8871-19, M5935-19, 8643-20). Human wound fluid material use was approved by the Ethics Committee at Lund University (LU 708-01 and LU 509-01). All donors have given informed consent. Human blood use was approved by the Ethics Committee at Lund University (permit no. 657–2008).

Supporting Information

Supporting Information is available from the Wiley Online Library or from the author.

Conflict of Interest

A.S. is one of the founders of in2cure AB, a company developing peptides for therapeutic applications. A patent application has been filed on materials with anti-inflammatory and/or anti-microbial properties.

Data Availability Statement

The data that support the findings of this study are available from the corresponding author upon reasonable request.

[1] a) T. G. Weiser, A. B. Haynes, G. Molina, S. R. Lipsitz, M. M. Esquivel, T. Uribe-Leitz, R. Fu, T. Azad, T. E. Chao, W. R. Berry, A. A. Gawande, *Bull. W. H. O.* **2016**, *94*, 201; b) G. P. Dobson, *Int. J. Surg.* **2020**, *81*, 47; c) T. G. Weiser, A. B. Haynes, G. Molina, S. R. Lipsitz, M. M. Esquivel, T. Uribe-Leitz, R. Fu, T. Azad, T. E. Chao, W. R. Berry, A. A. Gawande, *Lancet* **2015**, *385*, S11.

[2] B. M. Gillespie, E. Harbeck, M. Rattray, R. Liang, R. Walker, S. Latimer, L. Thalib, A. E. Andersson, B. Griffin, R. Ware, W. Chaboyer, *Int. J. Surg.* **2021**, *95*, 106136.

[3] a) C. D. Owens, K. Stoessel, *J. Hosp. Infect.* **2008**, *70*, 3; b) N. G. R. H. U. o. G. Surgery, *Lancet* **2021**, *398*, 1687; c) B. Allegranzi, S. B. Nejad, C. Combescure, W. Graafmans, H. Attar, L. Donaldson, D. Pittet, *Lancet* **2011**, *377*, 228; d) K. B. Kirkland, J. P. Briggs, S. L. Trivette, W. E. Wilkinson, D. J. Sexton, *Infect. Control Hosp. Epidemiol.* **1999**, *20*, 725.

[4] B. Allegranzi, P. Bischoff, S. De Jonge, N. Z. Kubilay, B. Zayed, S. M. Gomes, M. Abbas, J. J. Atema, S. Gans, M. Van Rijen, M. A. Boermeester, M. Egger, J. Kluytmans, D. Pittet, J. S. Solomkin, *Lancet Infect. Dis.* **2016**, *16*, e276.

[5] N. G. R. H. U. o. G. Surgery, *Lancet* **2022**, *400*, 1767.

[6] A. J. Mangram, T. C. Horan, M. L. Pearson, L. C. Silver, W. R. Jarvis, *Infect. Control Hosp. Epidemiol.* **1999**, *20*, 247.

[7] S. S. Magill, J. R. Edwards, W. Bamberg, Z. G. Beldavs, G. Dumyati, M. A. Kainer, R. Lynfield, M. Maloney, L. McAllister-Hollod, J. Nadle, S. M. Ray, D. L. Thompson, L. E. Wilson, S. K. Fridkin, Emerging Infections Program Healthcare-Associated Infections and Antimicrobial Use Prevalence Survey Team, *N. Engl. J. Med.* **2014**, *370*, 1198.

[8] a) S. V. Khiste, V. Ranganath, A. S. Nichani, *J. Periodontal Implant Sci.* **2013**, *43*, 130; b) C. G. Munton, C. I. Phillips, B. Martin, R. S. Bartholomew, I. Capperauld, *Br. J. Ophthalmol.* **1974**, *58*, 941.

[9] R. Karabulut, K. Sonmez, Z. Turkyilmaz, B. Bagbanci, A. C. Basaklar, N. Kale, *Indian J. Surg.* **2010**, *72*, 386.

[10] M. Byrne, A.l Aly, *Aesthetic Surg. J.* **2019**, *39*, S67.

[11] a) A. G. Gristina, J. L. Price, C. D. Hobgood, L. X. Webb, J. W. Costerton, *Surgery* **1985**, *98*, 12; b) S. Katz, M. Izhar, D. Mirelman, *Ann. Surg.* **1981**, *194*, 35.

[12] a) Y. Li, K. N. Kumar, J. M. Dabkowski, M. Corrigan, R. W. Scott, K. Nüsslein, G. N. Tew, *Langmuir* **2012**, *28*, 12134; b) G. Pulat, Z. Muganli, U. K. Ercan, O. Karaman, *J. Biomater. Appl.* **2023**, *37*, 1182.

[13] a) M. K. Diener, P. Knebel, M. Kieser, P. Schüler, T. S. Schiergens, V. Atanassov, J. Neudecker, E. Stein, H. Thielemann, R. Kunz, M. Von Frankenberg, U. Schernikau, J. Bunse, B. Jansen-Winkeln, L. I. Partecke, G. Prechtl, J. Pochhammer, R. Bouchard, R. Hodina, K. T. E. Beckurts, L. Leißner, H.-P. Lemmens, F. Kallinowski, O. Thomusch, D. Seehofer, T. Simon, A. Hyhlik-Dürr, C. M. Seiler, T. Hackert, C. Reissfelder, et al., *Lancet.* **2014**, *384*, 142; b) K. Ichida, H. Noda, R. Kikugawa, F. Hasegawa, T. Obitsu, D. Ishioka, R. Fukuda, A. Yoshizawa, S. Tsujinaka, T. Rikiyama, *Surgery.* **2018**, *164*, 91. c) W. P. Weber, W. R. Marti, M. Zwahlen, H. Misteli, R. Rosenthal, S. Reck, P. Fueglistaler, M. Bolli, A. Trampuz, D. Oertli, A. F. Widmer, *Ann. Surg.* **2008**, *247*, 918.

[14] A. Obermeier, J. Schneider, N. Harrasser, J. Tübel, H. Mühlhofer, D. Pförringer, C. V. Deimling, P. Foehr, B. Kiefel, C. Krämer, A. Stemberger, M. Schieker, R. Burgkart, R. Von Eisenhart-Rothe, *PLoS One* **2018**, *13*, e0190912.

[15] a) P. Papareddy, V. Rydengård, M. Pasupuleti, B. Walse, M. Mörgelin, A. Chalupka, M. Malmsten, A. Schmidtchen, *PLoS Pathog.* **2010**, *6*, e1000857; b) M. J. A. Van Der Plas, R. K. V. Bhongir, S. Kjellström, H. Siller, G. Kasetty, M. Mörgelin, A. Schmidtchen, *Nat. Commun.* **2016**, *7*, 11567.

[16] R. Saravanan, D. A. Holdbrook, J. Petrlova, S. Singh, N. A. Berglund, Y. K. Choong, S. Kjellström, P. J. Bond, M. Malmsten, A. Schmidtchen, *Nat. Commun.* **2018**, *9*, 2762.

[17] M. Puthia, M. Butrym, J. Petrlova, A. C. Strömdahl, M. Andersson, S. Kjellström, A. Schmidtchen, *Sci. Transl. Med.* **2020**, *12*, 26S.

[18] A.-C. Strömdahl, L. Ignatowicz, G. Petruk, M. Butrym, S. Wasserstrom, A. Schmidtchen, M. Puthia, *Acta Biomater.* **2021**, *128*, 314.

[19] a) F. C. Hansen, M. Kalle-Brune, M. J. A. Van Der Plas, A.-C. Strömdahl, M. Malmsten, M. Mörgelin, A. Schmidtchen, *J. Immunol.* **2015**, *194*, 5397; b) F. C. Hansen, A.-C. Strömdahl, M. Mörgelin, A. Schmidtchen, M. J. A. Van Der Plas, *Front. Immunol.* **2017**, *8*, 843.

[20] G. Petruk, J. Petrlova, F. Samsudin, R. D. Giudice, P. J. Bond, A. Schmidtchen, *Biomolecules.* **2020**, *10*, 1572.

[21] a) C. Del Amo, A. Perez-Valle, E. Perez-Zabala, K. Perez-Del-Pecho, A. Larrazabal, A. Basterretxea, P. Bully, I. Andia, *Int. J. Mol. Sci.* **2020**, *21*, 624; b) T. Maver, L. Gradisnik, D. M. Smrke, K. Stana Kleinschek, U. Maver, *AAPS PharmSciTech.* **2019**, *20*, 29.

[22] L. Ringstad, A. Schmidtchen, M. Malmsten, *Langmuir* **2006**, *22*, 5042.

[23] a) S. Malekkhaiat Häffner, L. Nyström, K. L. Browning, H. Mörck Nielsen, A. A. Strömstedt, M. J. A. Van Der Plas, A. Schmidtchen, M. Malmsten, *ACS Appl. Mater. Interfaces* **2019**, *11*, 15389; b) R. Nordström, L. Nyström, O. C. J. Andrén, M. Malkoch, A. Umerska, M. Davoudi, A. Schmidtchen, M. Malmsten, *J. Colloid Interface Sci.* **2018**, *513*, 141; c) R. Nordström, L. Nyström, H. Ilyas, H. S. Atreya, B. C. Borro, A. Bhunia, M. Malmsten, *Colloids Surf. A* **2019**, *565*, 8.

[24] S. Singh, M. Kalle, P. Papareddy, A. Schmidtchen, M. Malmsten, *Biomacromolecules* **2013**, *14*, 1482.

[25] L. D. Lozeau, M. W. Rolle, T. A. Camesano, *Colloids Surf., B* **2018**, *167*, 229.

[26] a) M. B. Giles, J. K. Y. Hong, Y. Liu, J. Tang, T. Li, A. Beig, A. Schwendeman, S. P. Schwendeman, *Nat. Commun.* **2022**, *13*, 3282; b) A. M. Sophocleous, K.-G. H. Desai, J. M. Mazzara, L. Tong, J.i-X. Cheng, K. F. Olsen, S. P. Schwendeman, *J. Controlled Release* **2013**, *172*, 662.

[27] K. Saleh, A. Schmidtchen, *Dermatol. Surg.* **2015**, *41*, 537.

[28] G. J. Reul Jr., *Am. J. Surg.* **1977**, *134*, 297.

[29] H. J. Busscher, H. C. Van Der Mei, G. Subbiahdoss, P. C. Jutte, J. J. A. M. Van Den Dungen, S. A. J. Zaat, M. J. Schultz, D. W. Grainger, *Sci. Transl. Med.* **2012**, *4*, 153rv10.

[30] R. Chua, S. K. Lim, C. F. Chee, S. P. Chin, L. V. Kiew, K. S. Sim, S. T. Tay, *Riv. Eur. Sci. Med. Farmacol.* **2022**, *26*, 828.

[31] H. P. Schweizer, *FEMS Microbiol. Lett.* **2001**, *202*, 1.

[32] M. T. E. Suller, *J. Antimicrob. Chemother.* **2000**, *46*, 11.

[33] N. Nadafpour, M. Montazeri, M. Moradi, S. Ahmadzadeh, A. Etemadi, *Front. Dent.* **2021**, *18*, 25.

[34] B. Elsolh, L. Zhang, S. V. Patel, *J. Gastrointest. Surg.* **2017**, *21*, 896.

[35] S. National Institute of Health Research Unit on Global, *Lancet Infect. Dis.* **2022**, *22*, 1242.

[36] Safety and Effectiveness of Consumer Antiseptics; Topical Antimicrobial Drug Products for Over-the-Counter Human Use, https://www.govinfo.gov/content/pkg/FR-2016-09-06/pdf/2016-21337.pdf (accessed: July 2023).

[37] Not approving triclosan as an existing active substance for use in biocidal products for product-type 1, https://eur-lex.europa.eu/eli/dec_impl/2016/110/oj (accessed: July 2023).

[38] T. Safety, Pharmacokinetics of Ascending Topical Doses of TCP-25 Applied to Epidermal Suction Blister Wounds, https://clinicaltrials.gov/ct2/show/NCT05378997 (accessed: July 2023).

[39] M. Champeau, J.-M. Thomassin, T. Tassaing, C. Jerome, *Macromol. Mater. Eng.* **2015**, *300*, 596.

[40] S. J. Marrink, H. J. Risselada, S. Yefimov, D. P. Tieleman, A. H. De Vries, *J. Phys. Chem. B* **2007**, *111*, 7812.

[41] H. Chandrasekhar, *J. Pharm. Sci. Res* **2017**, *9*, 2426.

[42] Y. K. Choi, S.-J. Park, S. Park, S. Kim, N. R. Kern, J. Lee, W. Im, *J. Chem. Theory Comput.* **2021**, *17*, 2431.

[43] J. Huang, A. D. Mackerell Jr., *J. Comput. Chem.* **2013**, *34*, 2135.

[44] S. Jo, T. Kim, V. G. Iyer, W. Im, *J. Comput. Chem.* **2008**, *29*, 1859.

[45] S. Nosé, *Mol. Phys.* **1984**, *52*, 255.

[46] M. Parrinello, A. Rahman, *J. Appl. Phys.* **1981**, *52*, 7182.

[47] U. Essmann, L. Perera, M. L. Berkowitz, T. Darden, H. Lee, L. G. Pedersen, *J. Chem. Phys.* **1995**, *103*, 8577.

[48] M. Pannuzzo, A. Felici, P. Decuzzi, *Biomacromolecules* **2022**, *23*, 4678.

[49] G. Bussi, D. Donadio, M. Parrinello, *J. Chem. Phys.* **2007**, *126*, 014101.

[50] A. Sali, T. L. Blundell, *J. Mol. Biol.* **1993**, *234*, 779.

[51] X. Periole, M. Cavalli, S.-J. Marrink, M. A. Ceruso, *J. Chem. Theory Comput.* **2009**, *5*, 2531.

[52] M. J. Abraham, T. Murtola, R. Schulz, S. Páll, J. C. Smith, B. Hess, E. Lindahl, *SoftwareX* **2015**, *1–2*, 19.

[53] W. Humphrey, A. Dalke, K. Schulten, *J. Mol. Graph.* **1996**, *14*, 33.

[54] O. Klementieva, C. Sandt, I. Martinsson, M. Kansiz, G. K. Gouras, F. Borondics, *Adv. Sci.* **2020**, *7*, 1903004.

[55] A. Paulus, S. Yogarasa, M. Kansiz, I. Martinsson, G. K. Gouras, T. Deierborg, A. Engdahl, F. Borondics, O. Klementieva, *Nanomedicine* **2022**, *43*, 102563.

[56] J. D. Morrisett, J. S. K. David, H. J. Pownall, A. M. Gotto Jr., *Biochemistry* **1973**, *12*, 1290.

[57] K. Lundqvist, H. Herwald, A. Sonesson, A. Schmidtchen, *Thromb. Haemost.* **2004**, *92*, 281.